

# Flight performance of the Early Cretaceous bird *Confuciusornis sanctus*: evidence from an exceptionally preserved fossil

Capacidad de vuelo del ave del Cretácico Inferior *Confuciusornis sanctus*: evidencias desde un fósil excepcionalmente preservado

Luis M. CHIAPPE , Francisco J. SERRANO , Stephanie ABRAMOWICZ  & Ursula B. GÖHLICH 

**Abstract:** The Chinese Early Cretaceous *Confuciusornis sanctus* is the most abundant Mesozoic bird and a model species for studies of early avian evolution. While previous investigations were largely focused on aspects of the anatomy, taxonomy and systematics, and life history and ecology of this bird, there has been minimal research on its flight properties. Our study centers on a well-preserved specimen with exquisite details of its plumage. NHMW 1997z0112/0001 affords novel information on aspects of its skeletal morphology, particularly from the axial and appendicular skeletons, and its plumage provides the opportunity to quantify key flight-related variables including, wingtip, wing chord, body mass, wingspan, and wing area. We use these parameters to provide a quantitative assessment of the flight properties of *C. sanctus*. Most previous studies have suggested that this species was unable to achieve prolonged flights. However, our results indicate that the capacity for this bird to perform prolonged flights cannot be discarded, given that our data shows it might have been able to combine periods of flapping with periods of efficient low-speed gliding. Specifically, our results indicate that while having slightly less capacity than modern gliding birds, the gliding capacity of *C. sanctus* would have been significantly higher than that of modern short-term fliers such as land fowl. On the basis of these inferences, we conclude that *C. sanctus* could fly efficiently for prolonged periods of time when using a combination of flapping and gliding periods.

**Resumen:** *Confuciusornis sanctus* del Cretácico Inferior de China es el ave mesozoica más abundante y una especie modelo para el estudio de la evolución temprana de las aves. Los estudios previos se han enfocado principalmente en aspectos de su anatomía, taxonomía, sistemática, crecimiento y ecología, pero sus propiedades de vuelo apenas se han investigado. Este estudio se centra en un espécimen muy bien conservado que presenta un nivel de detalle excepcional en su plumaje. NHMW 1997z0112/0001 proporciona nueva información sobre la morfología esquelética, particularmente del esqueleto axial y apendicular, y su plumaje proporciona la oportunidad de cuantificar variables clave relacionadas con el vuelo, como la punta del ala, la cuerda alar, la masa corporal, la envergadura y la superficie alar. Aquí usamos estos parámetros para evaluar cuantitativamente la capacidad de vuelo de *C. sanctus*. Muchos estudios previos han sugerido que esta especie era incapaz de llevar a cabo vuelos prolongados. Sin embargo, nuestros resultados indican que su capacidad para realizar vuelos largos no puede ser descartada, ya que nuestras reconstrucciones aerodinámicas evidencian que durante su vuelo pudo ser capaz de combinar periodos de aleteo con periodos de planeo a baja velocidad. Específicamente, los resultados muestran que *C. sanctus* tuvo una capacidad de planeo ligeramente menor que las aves planeadoras modernas, pero significativamente superior a las aves modernas adaptadas a vuelos cortos como las gallináceas. En base a estas inferencias, concluimos que *C. sanctus* pudo volar eficientemente durante periodos prolongados, usando una combinación de fases de aleteo y planeo.

Received: 7 June 2023

Accepted: 11 October 2023

Published: 2 November 2023

## Corresponding authors:

Luis M. Chiappe

[lchiappe@nhm.org](mailto:lchiappe@nhm.org)

Francisco J. Serrano

[fjsa@uma.es](mailto:fjsa@uma.es)

## Keywords:

Aves

Mesozoico

Evolution

Palaeontology

Aerodynamics

## Palabras-clave:

Aves

Mesozoico

Evolución

Paleontología

Aerodinámica

## INTRODUCTION

*Confuciusornis sanctus* (Hou *et al.*, 1995) is the most abundant Mesozoic avian species and a model for the evolution of early birds (Chiappe & Meng, 2016), of which anatomy was monographed by Chiappe *et al.* (1999). Previous studies on this iconic taxon have covered aspects of its anatomy (Chiappe *et al.*, 1999;

Elzanowski *et al.*, 2018; Falk *et al.*, 2019; Wu *et al.*, 2021), taxonomy and systematics (Hou *et al.*, 1995, 1999; Chiappe *et al.*, 1999; Marugán-Lobón *et al.*, 2011; Wang *et al.*, 2018), plumage (Chiappe *et al.*, 1999; O' Connor *et al.*, 2012; Falk *et al.*, 2016; Pan *et al.*, 2016; Li *et al.*, 2018), life history (Chiappe *et al.*, 2008; Peters

& Peters, 2009; Marugán-Lobón *et al.*, 2011; Chinsamy *et al.*, 2013, 2020; Marugán-Lobón & Chiappe, 2022), and ecology (Martin *et al.*, 1998; Dalsätt *et al.*, 2006) but there has been minimal research focusing on the flight properties of *C. sanctus* and its relatives. Previous interpretations of the aerial capacity of these birds have been largely based on qualitative studies of *C. sanctus* (Zhou & Farlow, 2001; Peters & Peters, 2009; Nudds & Dyke, 2010; Falk *et al.*, 2016; Pittman *et al.*, 2022). While these studies have regularly concluded that *C. sanctus* had some sort of aerial locomotion, these aerodynamic interpretations have ranged from having minimal flight capabilities (Nudds & Dyke, 2010) to being able to perform a degree of gliding (Senter, 2006; Wang *et al.*, 2019) or soaring (Peters & Ji, 1999), or to conduct powered flight but limited to short periods of time (Falk *et al.*, 2016). What all these studies have in common is the assumption that *C. sanctus* was unable to perform prolonged periods of flight (although Wang *et al.* (2022) recently suggested that the basal confuciusornithid *Eoconfuciusornis zhengi* was adapted for fast, long-distant flight).

The present study focuses on a well-preserved, fully feathered specimen (NHMW 1997z0112/0001) of *Confuciusornis sanctus* (Figs. 1, 2) housed at the Naturhistorisches Museum Wien, Austria. NHMW 1997z0112/0001 affords information on several aspects of its skeletal anatomy not published previously but most importantly, its exceptionally well-preserved wing plumage provides the basis for a quantitative assessment of its flight properties. Here we recover key parametric data germane to the flight capabilities of *C. sanctus* and, for the first time, test hypotheses about the aerial performance of this species through flight modeling. It is important to highlight that there is growing evidence of varying flight modes among confuciusornithids (Wang *et al.*, 2022). Consequently, while our study provides a reliable framework for understanding flight performance in *C. sanctus*, our conclusions need to be treated with caution if extrapolated to other confuciusornithids, particularly for taxa with different wing outlines such as *Eoconfuciusornis zhengi*, which appears to lack the distinct elongation of the distal primaries of *C. sanctus*.

## MATERIALS AND METHODS

### Provenance, Taphonomy, and Preservation

NHMW 1997z0112/0001 was acquired by the Naturhistorisches Museum Wien (NHMW) in 1997 (purchased from R. Henzel (Celle, Germany) and shortly after it was mechanically prepared by Franz Topka, a palaeontological preparator at this institution (Fig. 1)). The Museum's correspondence indicates that negotiations were in place in March 1997, which in turn indicates that the specimen was discovered in 1996 or earlier. While the specific locality was not documented in the correspondence, this specimen was

likely collected from Sihetun locality, as this locality was the prime source for fossils of *Confuciusornis sanctus* at these years. NHMW 1997z0112/0001 has been on display at the Naturhistorisches Museum Wien for years and it remains available for scientific study by qualified researchers. Currently, NHMW is engaged in conversations about how to remediate issues related to the provenance of the specimen.

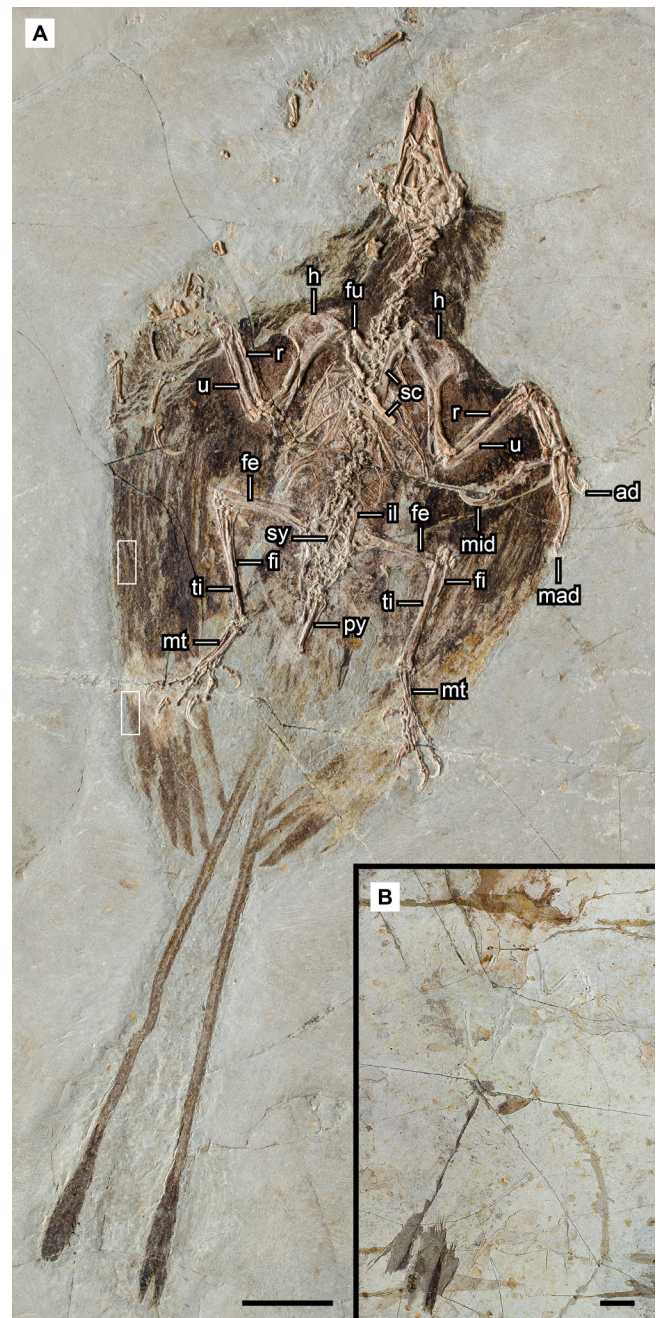


**Figure 1.** A–B, *Confuciusornis sanctus* NHMW 1997z0112/0001; **A**, full specimen; **B**, original slab prior to mechanical preparation. Rectangular boxes (A) demarcate portions of outer primaries in which rachis width was estimated (see text). **ad**, alular digit; **fe**, femur; **fi**, fibula; **fu**, furcula; **h**, humerus; **il**, ilium; **mad**, major digit; **mid**, minor digit; **mt**, metatarsus; **py**, pygostyle; **r**, radius; **sc**, scapula; **sy**, synsacrum; **ti**, tibiotarsus; **u**, ulna; scale bar = 5 cm.

NHMW 1997z0112/0001 is nearly complete and fully articulated, its skeleton exposed primarily in dorsal view. Exquisite evidence of its plumage, revealing portions of the rachises and vanes, is preserved throughout the body and including its neck, both wings, trunk, and tail. Remnants of soft tissues representing wing patagia and muscle packages surrounding the femur and tibiotarsus are visible under ultraviolet illumination (Fig. 2). Keratinous sheaths covering the unguis phalanges, both manual and pedal, are preserved. The specimen also includes the full extent of its wings and a complete set of caudal ornamental feathers.

### Anatomical description

Examination of the anatomy and morphology of NHMW-1997z0112/0001 was performed using binocular magnifier and high-resolution images under UV light.

### Reconstruction of the feathered wing outline

The outline of NHMW-1997z0112/0001 in flight was reconstructed using photographs of the specimen (taken under normal and ultraviolet light). The photos were stacked and scaled in superimposed layers in Adobe Illustrator and used as reference to trace the preserved primary and secondary feathers, and feather-bearing bones, and to reposition them as they would have been in a fully-spread wing.

When tracing the wing plumage, solid lines were used to trace over areas of the specimen that are well-preserved and unambiguous to observe (Fig. 3). Dashed lines were used in areas where the feather outlines were inferred. "Inferred" refers to portions of a feather that are obscured, incomplete or unclear to observe in the specimen that have been drawn according to the most reasonable interpretation (e.g., connecting two segments of a rachis) and are supported by observations made from photographs of other specimens of *Confuciusornis sanctus* (STM13-55, STM13-170, STM13-62, STM13-45, STM13-133, DNHM-2151, BMNHC-PH-987). Lines were drawn connecting rachises to points on the feather-bearing bones, and these points were used as pivots for rotating the feathers when repositioning them for the reconstruction (Figs. 3, 4) so that the feathers would maintain their lengths. In order to straighten the curvature of a given rachis for the reconstruction, while maintaining its original length, the line of the original rachis tracing was cut into segments and repositioned end to end in a straighter arrangement.

Feather tips can be seen preserved on the right wing of NHMW-1997z0112/0001 around where the first primary and first secondary would be expected to be (Fig. 3). However, it is not clear how many there are and whether these feather tips belong to the primaries or secondaries. Rachis lines were drawn from the wing tips to show a version of two possibilities (Fig. 3): they were drawn as two suspected primaries with dashed

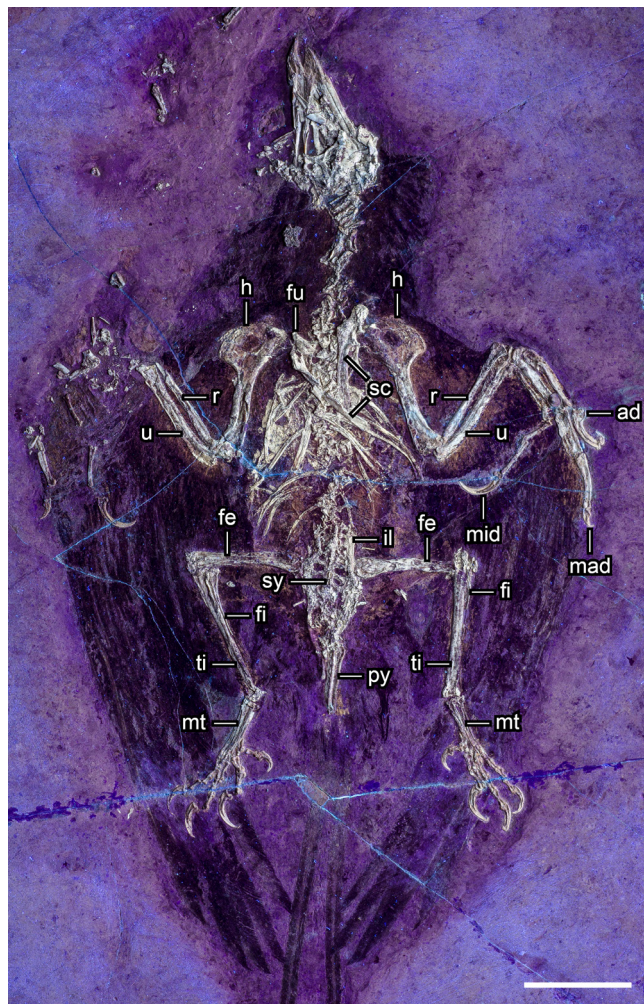
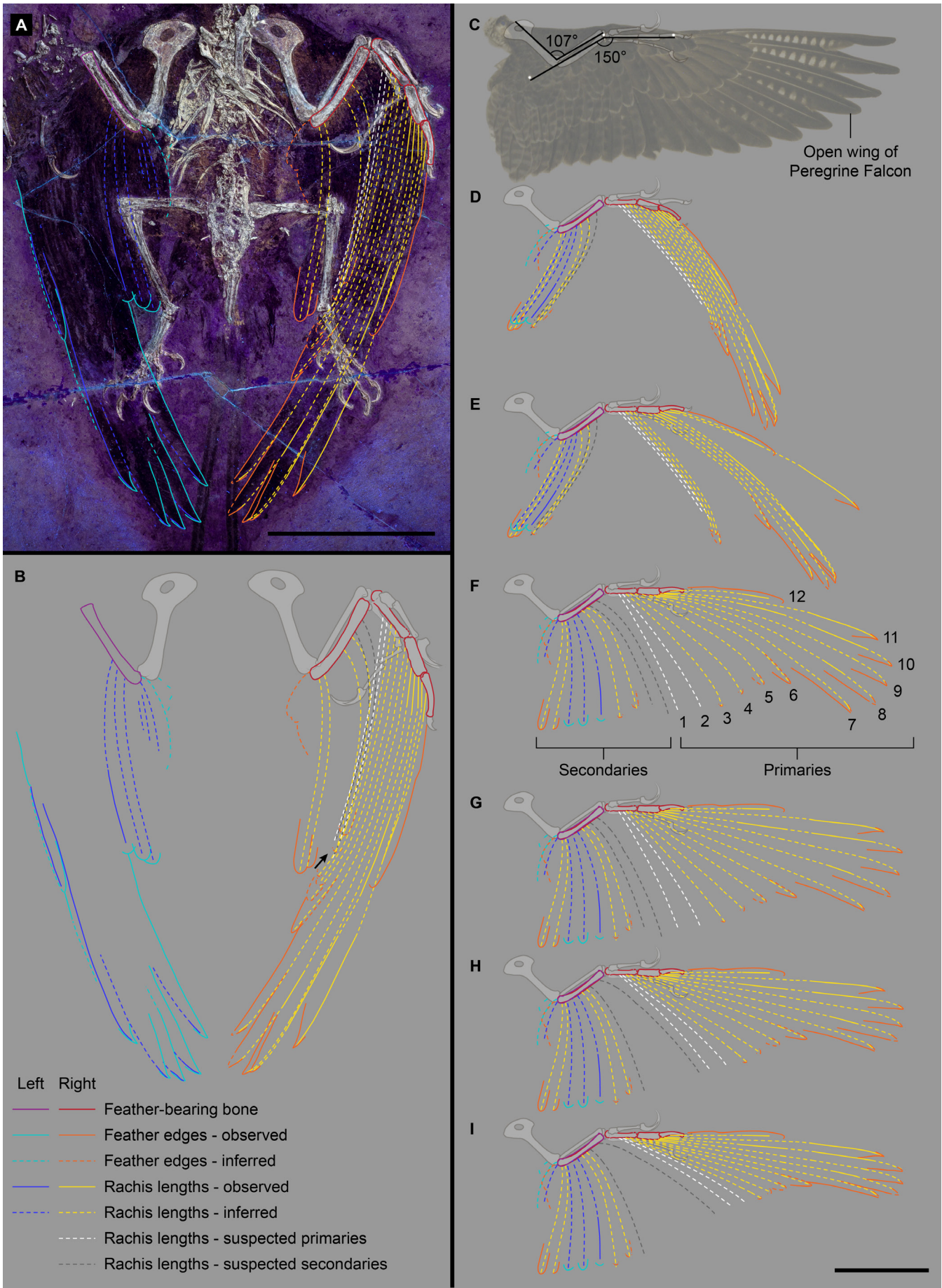


**Figure 2.** NHMW 1997z0112/0001 under UV illumination. **ad**, alular digit; **fe**, femur; **fi**, fibula; **fu**, furcula; **h**, humerus; **il**, ilium; **mad**, major digit; **mid**, minor digit; **mt**, metatarsus; **py**, pygostyle; **r**, radius; **sc**, scapula; **sy**, synsacrum; **ti**, tibiotarsus; **u**, ulna; scale bar = 5 cm.

white lines connecting them to the major metacarpal, and they were also drawn as two suspected secondaries with two gray dashed lines connecting them to the ulna (Fig. 3). Nonetheless, based on how these feathers fit in the reconstruction, we consider that they are likely primaries, thus supporting the number of primaries (and their locations) in an interpretation of the soft tissue preserved in specimens STM13-55 and STM13-170; as seen in Figure 3F–3G, the longer of the two gray rachises we drew seems too long as a secondary but in Figure 3H–3I they look reasonable. Consequently, we reconstructed three models that span the range of these alternatives for outline reconstruction (Fig. 4): OR1, OR2 and OR3.

The position of the bones in the fully extended forelimb reconstruction of NHMW-1997z0112/0001 references the maximum extension (*i.e.*, maximum elbow angle) of the open wing of a Peregrine Falcon, *Falco peregrinus* (UWBM 78842) (Fig. 3C). The forelimb bones of NHMW-1997z0112/0001 were repositioned into an arrangement similar to the falcon; 150° angle at the wrist and 107° angle at the elbow (Fig. 3C).



The same method was used to reconstruct the rest of the outline of the specimen in flight (Fig. 4). The reconstruction uses the same distance between the right and left humerus as preserved in the fossil and maintains the relationships preserved for the head, neck and tail including the shapes and lengths of the short rectrices surrounding the pygostyle and the pair of long rachis-dominated feathers (RDFs), and the angle formed between them.

### Quantitative Aerodynamic Analysis

Measurements of NHMW 1997z0112/0001 were obtained directly from the fossil using digital calipers (Tab. 1). The exceptional preservation of its forelimb and wing feathers afforded accurate measurements of key variables for inferring flight performance, including wingtip (distance from the end of the second phalanx of major digit to the feathered wingtip) and the wing chord (craniocaudal breadth of the wing at wrist level) (Fig. 4). The body mass ( $M_b$ ) of NHMW 1997z0112/0001 (0.615 Kg) was estimated using a multiple regression equation developed specifically for confuciusornithids (Serrano et al., 2015), and the values of wingspan ( $B$ ) and wing area ( $S_L$ ) were obtained from multiple regressions (MR) equations based on wing bones and flight feathers (MR-B1 and MR-SL-Conf in Serrano et al., 2017) (Tab. 2). These multiple regressions were derived from a broad (taxonomically and ecologically) sample of extant birds, and the limb variables included in the equations were selected when the values for fossils fell within the range of the modern bird sample (i.e., if the value of a particular fossil scored outside of the 95% confidence interval of modern birds, this variable was discarded). Such an approach reduced the potential errors associated with stem-ward inference and ecological differences (see detailed method in Serrano et al., 2015, 2017). In addition, the values of wingspan ( $B$ ) and wing area ( $S_L$ )

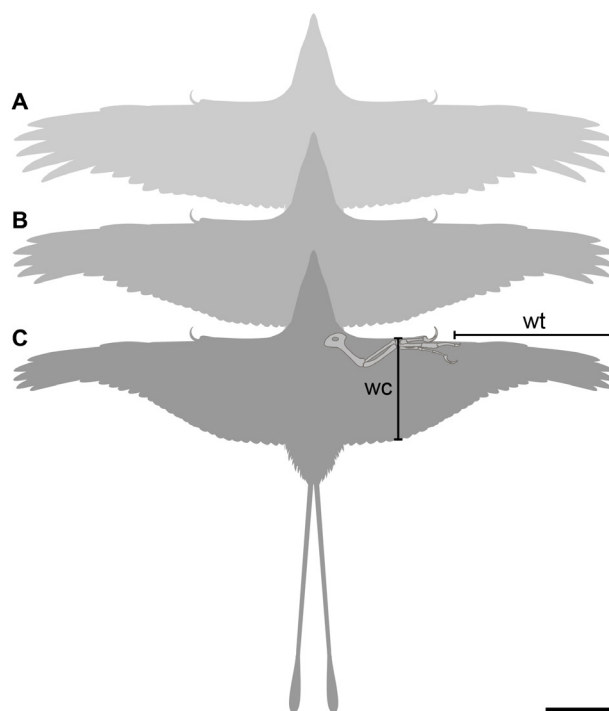


**Figure 4.** A–C, *Confuciusornis sanctus*, NHMW 1997z0112/0001; **A**, spread wing reconstruction based on the approach outlined in Figure 3G (OR1); **B**, spread wing reconstruction based on the approach outlined in Figure 3H (OR2); **C**, spread wing reconstruction based on the approach outlined in Figure 3I (OR3). Abbreviations: **wc**, wing cord; **wt**, wing tip; scale bar = 10 cm.

for the reconstructed wing of NHMW 1997z0112/0001 were measured from the reconstructed wing outline (see above) using Image J 1.51jj8 software (<http://imagej.nih.gov/ij>). The wing loading ( $WL$ ) and aspect ratio ( $AR$ ) of NHMW 1997z0112/0001 were calculated using the following equations:  $WL = M_b^{2/3}/S_L$  and  $AR = B^2/S_L$ . All analyses and aerodynamic modeling of

[Figure on previous page](#)

**Figure 3.** A–I, Stages of the process used to reconstruct the wing of NHMW-1997z0112/0001. Key depicts a range of confidence in the reconstruction of the wing plumage: ‘Inferred’ refers to portions of an incomplete feather drawn according to the most reasonable interpretation (e.g., connecting two segments of a rachis). ‘Suspected’ is used for instances when there is difficulty outlining individual feathers and/or their attachment position is uncertain (e.g., first primaries and first secondaries); **A**, UV photograph of NHMW-1997z0112/0001 with superimposed tracings of feather outlines, rachises and forelimb bones; **B**, tracings of feather outlines, rachises and forelimb bones (black arrow points at an area that would be expected to include the first primaries and/or the first secondaries but that is partially obscured by the ankle bones); **C**, the traced bones of the forelimb of NHMW 1997z0112/0001 superimposed over a photograph of the open wing of a Peregrine Falcon (UWBM 78842), the forelimb bones of NHMW 1997z0112/0001 have been re-positioned similar to what is seen in the falcon (i.e., 150° angle at the wrist and 107° angle at the elbow); **D**, original tracings of the feathers and feather-bearing bones from (B) are placed onto the newly positioned forelimb by overlaying and aligning the tracings of the feather-bearing bones and keeping the feathers anchored to them in their original position; **E**, bones of the hand are straightened to match the bones in the reconstructed forelimb, and feather tracings are moved with the bones they are anchored to; **F**, feathers, retaining the original curvatures of the rachises drawn in the tracing interpretation of the specimen (B), are spread; **G**, rachises are straightened and the feathers are positioned to be similar to the arrangement and spacing of the falcon feathers in the reference photo (C); **H**, feathers are positioned in an arrangement/spacing that is intermediate to versions (G) and (I), the first primary is placed at an angle in between what is used in (G) and (I); **I**, rachises of the longest primaries are slightly more curved than in (H) and are positioned in a tighter arrangement. Note that while we do not have certainty about the first two primaries shown with white dashed lines, their likely existence is supported by an interpretation of soft tissue preserved in STM13-55 and STM13-170; scale bars = 10 cm (falcon wing is not in scale).

NHMW 1997z0112/0001 were conducted using the two above-mentioned approaches for estimating  $B$  and  $S_L$ : outline reconstructions (OR1, OR2 and OR3) (Fig. 4) and multiple regressions (MR).

The power available from aerobic metabolism ( $P_{av}$ ) was calculated using an oxygen consumption rate ( $V_{O_2}$ , mL/min) in which 1 mL  $O_2$ /min generates 20.1 W during aerobic activity (Schmidt-Nielsen, 1997). Values of  $V_{O_2}$  were estimated for NHMW 1997z0112/0001 using equation 1, from (Bishop & Butler, 2015).

$$(1) V_{O_2} = 160 M_b 0.74$$

By assuming a conversion efficiency of 0.2 from the total metabolic power input to  $P_{av}$  (Tucker, 1973; Pennycuick, 2008), and translating minutes into seconds—as values from eq. 1 were derived from  $V_{O_2}$  measured in mL/min—the  $P_{av}$  at modern conditions was calculated using eq. 2.

$$(2) P_{av} = 20.1 \times 0.2 / 60 V_{O_2}$$

$$P_{av} = 0.067 V_{O_2}$$

Values of  $P_{av}$  for NHMW 1997z0112/0001 were adjusted to the atmospheric  $O_2$  concentration (AOC) at 125 Myr (Ward & Berner, 2011)—the approximated age of the Sihetun site—using eqs. 3 and 4 from (Serrano et al., 2019).

$$(3) \% \Delta AOC = (AOC (125 \text{ Myr}) - AOC (\text{today})) \times 100 / AOC (\text{today})$$

$$(4) P_{av} = (0.067 V_{O_2} \cdot \% \Delta AOC) + 0.067 V_{O_2}$$

We constructed a power curve—theoretical relationship between mechanical power output necessary for sustained flapping flight ( $P_{mec}$ ) and forward speed ( $V_t$ )—for NHMW 1997z0112/0001 using the software Flight v. 1.24 (<http://www.bio.bristol.ac.uk/people/pennycuick.htm>) (Pennycuick, 2008). The values of  $P_{mec}$  for a range of velocities  $V_t$  were calculated according to eq. 5, as the summation of the induced power ( $P_{ind}$ ; eq. 6, where  $k$  is the induced power factor and  $g$  is the gravity acceleration), the parasite power ( $P_{par}$ ; eq. 7, where  $S_b$  is the frontal area of the body and  $C_{Db}$  is the body drag coefficient), and the profile power ( $P_{pro}$ ; eq. 8, where  $V_{mp}$  is the minimum power speed and  $C_{pro}$  is the profile power constant).

$$(5) P_{mec} = P_{ind} + P_{par} + P_{pro}$$

$$(6) P_{ind} = 2 k (M_b g)^2 / V_t \pi B^2 \rho_{air}$$

$$(7) P_{par} = \rho_{air} V_t^3 S_b C_{Db} / 2$$

$$(8) P_{pro} = (2k (M_b g)^2 / V_{mp} \pi B^2 \rho_{air} + \rho_{air} V_{mp}^3 S_b C_{Db} / 2) C_{pro} / (B^2 / S_L)$$

These calculations require assumptions for some of the components, particularly in fossils (Serrano et al., 2018). For example,  $k$ —parameter that accounts for any deviations from elliptical distribution of the lift across the wingspan—was set at  $k = 1.2$ , a value typically observed in aircrafts, while  $C_{pro}$  was fixed

**Table 1.** Measurements (in mm) of NHMW 1997z0112/0001 obtained directly from the fossil using digital calipers.

Variable	Right	Left
Skull, length		67.7
Pygostyle, length		30.0
Humerus, length	65.2	65.1
Humeral head, major axis	-	8.5
Humerus, midshaft width	7.1	7.7
Humerus, distal maximum width	13.1	-
Deltpectoral crest, length	26.3	26.1
Ulna, length	56.5	-
Ulna, proximal maximum width	6.6	7.9
Ulna, midshaft width	5.0	5.3
Radius, length	54.1	-
Radius, midshaft width	2.8	3.5
Carpometacarpus, length (semilunate to joint with major digit)	32.3	-
Carpometacarpus, proximal maximum width	14.1	-
Carpometacarpus, distal maximum width	8.0	-
Alular metacarpal, length	10.5	-
Major metacarpal, length	32.5	-
Minor metacarpal, length	24.8	-
Major metacarpal, midshaft width	4.4	-
Alular digit ph1, length	24.7	-
Alular digit ph2, length	16.0	-
Major digit ph1, length	22.9	-
Major digit ph2, length	26.0	-
Major digit ph3, length	5.7	-
Minor digit ph1, length	5.7	-
Minor digit ph2, length	14.8	16.1
Minor digit ph3, length	19.0	19.1
Minor digit ph4, length	14.2	13.2
Femur, length	-	53.8
Femur, midshaft width	5.6	5.4
Tibiotarsus, length	68.1	66.6
Metatarsal I, length	7.5	-
Metatarsal II, length	26.0	-
Metatarsal III, length	29.8	-
Metatarsal IV, length	28.5	-
Metatarsal V, length	-	6.0
Pedal digit 1 ph1, length	6.0	-
Pedal digit 1 ph2, length	6.3	-
Pedal digit 2 ph1, length	8.1	-
Pedal digit 2 ph2, length	10.0	-
Pedal digit 2 ph3, length	10.0	-
Pedal digit 3 ph1, length	10.0	-
Pedal digit 3 ph2, length	7.8	-
Pedal digit 3 ph3, length	7.4	-
Pedal digit 3 ph4, length	8.9	-
Pedal digit 4 ph1, length	6.2	-
Pedal digit 4 ph2, length	5.1	-
Pedal digit 4 ph3, length	5.2	-
Pedal digit 4 ph4, length	6.4	-
Pedal digit 4 ph5, length	8.0	-
Maximum chord from wrist to wingtip	296	-
Length of longest primary feather	238.8	-
Wing chord at wrist level	172.1	166.2

at 8.4 to make  $P_{pro}$  proportional to the wing area (Pennycuick, 2008). The  $S_b$  of NHMW 1997z0112/0001 was calculated from its allometric relationship with the  $M_b$  observed in modern birds (eq. 9) (Pennycuick, 2008).  $C_{Db}$  was obtained from this  $S_b$ , and from the equivalent flat plate area ( $A$ ) (eq. 10). For estimating

**Table 2.** Values (means and uncertainty ranges) derived from the two analytical approaches (see Materials and Methods), multiple regressions (MR) and outline reconstructions (OR). Abbreviations: **AR**, aspect ratio; **B**, wingspan; **C<sub>Db</sub>**, body drag coefficient; **M<sub>b</sub>**, body mass; **N<sub>max</sub>**, maximum value of lift-to-drag ratio; **P<sub>av</sub>**, power available from aerobic metabolism; **P<sub>mec</sub>**, mechanical power output necessary for sustained flapping flight; **RWL**, relative wing loading; **S<sub>b</sub>**, frontal area of the body; **S<sub>L</sub>**, wing area; **V<sub>bg</sub>**, best glide speed; **V<sub>mp</sub>**, minimum power speed; **V<sub>mr</sub>**, cruising speed; **V<sub>O2</sub>**, oxygen consumption rate; **V<sub>z</sub>**, sinking speed; **WL**, wing loading.

	MR		OR1		OR2		OR3	
	mean	range	mean	range	mean	range	mean	range
<b>M<sub>b</sub> (Kg)</b>	0.615	0.511–0.719	0.615	0.511–0.719	0.615	0.511–0.720	0.615	0.511–0.721
<b>B (m)</b>	0.862	0.839–0.884	0.881	0.881	0.881	0.881	0.881	0.881
<b>S<sub>L</sub> (m<sup>2</sup>)</b>	0.112	0.104–0.120	0.101	0.101	0.094	0.094	0.084	0.084
<b>AR</b>	6.6	6.5–6.7	7.7	7.7	8.3	8.3	9.3	9.3
<b>RWL</b>	6.5	6.1–6.7	7.2	6.3–8.0	7.7	6.8–8.6	8.6	7.6–9.8
<b>S<sub>b</sub> (cm<sup>2</sup>)</b>	58.8	52.0–65.3	58.8	52.0–65.3	58.8	52.0–65.3	58.8	52.0–65.5
<b>C<sub>Db</sub></b>	0.190	0.183–0.201	0.171	0.154–0.194	0.159	0.143–0.180	0.143	0.129–0.163
<b>V<sub>O2</sub> (ml O<sub>2</sub>/ min)</b>	111.7	97.4–125.4	111.7	97.4–125.4	111.7	97.4–125.5	111.7	97.4–125.6
<b>P<sub>av</sub> (W)</b>	6.2	5.4–6.9	6.2	5.4–6.9	6.2	5.4–6.10	6.2	5.4–6.11
<b>V<sub>mp</sub> (m/s)</b>	11.2	10.5–11.8	10.6	9.6–11.4	10.8	9.8–11.6	11.9	10.8–12.11
<b>V<sub>mr</sub> (m/s)</b>	18.7	17.5–19.6	17.4	15.9–18.7	17.5	16.1–18.9	19	17.4–20.7
<b>P<sub>mec</sub> at V<sub>mp</sub> (W)</b>	8.48	6.5–10.6	5.94	4.50–7.51	5.61	4.25–7.09	6.43	4.87–8.14
<b>P<sub>mec</sub> at V<sub>mr</sub> (W)</b>	10.8	8.3–13.4	7.55	5.74–9.49	7.09	5.43–8.95	8.07	6.1–10.4
<b>N<sub>max</sub></b>	12.9	12.7–13.0	14.1	14.1	14.8	14.7–14.8	15.7	15.7
<b>V<sub>bg</sub> (m/s)</b>	11.1	10.4–11.6	11.2	10.2–12.1	11.4	10.4–12.4	11.7	10.7–12.9
<b>V<sub>z</sub> at N<sub>max</sub> (m/s)</b>	0.86	0.80–0.91	0.79	0.72–0.86	0.77	0.71–0.84	0.74	0.68–0.83
<b>minimum V<sub>z</sub> (m/s)</b>	0.71	0.66–0.75	0.65	0.60–0.71	0.64	0.58–0.69	0.62	0.56–0.69

**Table 3.** Values of aerodynamic parameters of different species of modern birds necessary to depict the gliding performance graphs of Figure 13. The predominant aerial strategy of each species is also indicated.

Species	Specimen/Source	Aerial strategy	BM (kg)	B (m)	S <sub>L</sub> (m <sup>2</sup> )	AR	N <sub>max</sub>	V <sub>bg</sub> (m/s)	V <sub>z</sub> at N <sub>max</sub> (m/s)	V <sub>z</sub> min (m/s)
<i>Accipiter gentilis</i>	UWBM 80189	Continental soaring-gliding	0.768	1.060	0.180	6.2	12.4	9.8	0.79	0.65
<i>Circus aeruginosus</i>	UWBM 56456	Continental soaring-gliding	0.560	1.054	0.164	6.8	13.0	8.6	0.66	0.54
<i>Hieraaetus pennatus</i>	Bruderer et al. 2010	Continental soaring-gliding	0.595	1.160	0.200	6.7	13.0	8.0	0.62	0.51
<i>Falco peregrinus</i>	UWBM 78842	Continental soaring-gliding	0.699	1.000	0.125	8.0	14.4	10.5	0.73	0.60
<i>Bubo virginianus</i>	UWBM 72511	Continental soaring-gliding	0.832	1.340	0.290	6.2	12.3	8.0	0.65	0.53
<i>Ninox novaeseelandiae</i>	UWBM 57397	Continental soaring-gliding	0.500	0.904	0.136	6.0	12.1	9.2	0.76	0.62
<i>Corvus corone</i>	UWBM 56471	Continental soaring-gliding	0.575	0.966	0.160	5.8	11.9	9.1	0.77	0.63
<i>Puffinus diomedea</i>	Viscor and Fuster 1987	Oceanic soaring-gliding	0.572	1.211	0.128	11.5	17.9	8.5	0.48	0.40
<i>Fulmarus glacialis</i>	Viscor and Fuster 1987	Oceanic soaring-gliding	0.725	1.090	0.102	11.6	18.0	10.7	0.59	0.50
<i>Stercorarius pomarinus</i>	UWBM 59608	Oceanic soaring-gliding	0.571	1.180	0.156	8.9	15.4	8.2	0.53	0.44
<i>Larus fuscus</i>	Bruderer et al. 2010	Oceanic soaring-gliding	0.797	1.340	0.190	9.5	15.9	8.7	0.55	0.45
<i>Larus argentatus</i>	Bruderer et al. 2010	Oceanic soaring-gliding	0.705	1.350	0.200	9.1	15.6	8.0	0.51	0.43
<i>Podiceps cristatus</i>	UWBM 56440	Short-term fliers	0.985	0.750	0.064	8.8	15.3	17.0	1.11	0.92
<i>Uria aalge</i>	UWBM 79468	Short-term fliers	0.925	0.722	0.061	8.5	15.0	17.0	1.14	0.94
<i>Centropus milo</i>	UWBM 66047	Short-term fliers	0.790	0.770	0.171	3.5	8.5	11.7	1.38	1.12
<i>Fulica atra</i>	UWBM 56581	Short-term fliers	0.825	0.736	0.075	7.2	15.1	15.1	1.12	0.92
<i>Lagopus lagopus</i>	UWBM 58896	Short-term fliers	0.575	0.628	0.063	6.3	12.4	14.3	1.15	0.94
<i>Megapodius freycinet</i>	UWBM 60327	Short-term fliers	0.860	0.765	0.125	4.7	10.3	13.3	1.29	1.05
<i>Porphyrio porphyrio</i>	UWBM 63060	Short-term fliers	0.715	0.727	0.093	5.7	11.7	13.4	1.15	0.94

A, we followed the approach from Taylor and Thomas (2014), who assumed a body drag equivalent to the drag on a flat plate with 1% of the area of the wings (eq. 11). Rearranging equations 10 and 11, C<sub>Db</sub> was estimated using eq. 12:

$$(9) S_b = 0.00813 M_b^{0.666}$$

$$(10) A = S_b C_{Db}$$

$$(11) A = 0.01 S_L$$

$$(12) C_{Db} = (0.01 S_L) / S_b$$

The cruising speed (V<sub>mr</sub>)—the speed with minimum cost of transport—was calculated as the speed where the tangent to the power curve intersects with the origin of the speed–power plot (Rayner, 1999).

The dynamics of gliding were studied through the glide polar graph that relates the sinking speeds (V<sub>z</sub>) to a range of forward speed V<sub>t</sub>. The sinking speed (V<sub>z</sub>) was calculated using eq. 13, where D is the total aerodynamic drag resulting from the sum of the induced, parasite, and profile drags (Pennycuick, 2008).

$$(13) V_z = D V_t / M_b g$$

Gliding birds reduce wingspan as they increase speed, by flexing the elbow and wrist joints. To calculate  $V_z$ , we assumed that wingspan decreases as a linear function of speed based on a wind tunnel study of a gliding jackdaw (Rosén & Hedenström, 2001). We also used an induced drag factor of 1.0 (Taylor et al., 2016). Following Pennycuik (2008), the lift-to-drag ratio ( $N$ ) was calculated at different speeds from the relation between horizontal and vertical speeds (i.e.,  $V/V_z$ ), and its maximum value ( $N_{max}$ ) was taken to indicate the best glide speed ( $V_{bg}$ ). The values of gliding performance calculated for NHMW 1997z0112/0001 were compared with those values in modern birds with different flight strategies (Tab. 3). We ran one-way ANOVA and post-hoc Bonferroni to test differences in  $V_z$  at  $N_{max}$  using IBM SPSS Statistic v.20 (<https://www.ibm.com/products/software>).

### Institutional Acronyms

**BMNH-CH**, Beijing Museum of Natural History (Beijing, China); **DNHM**, Dalian Natural History Museum (Dalian, China); **IVPP**, Institute of Vertebrate Paleontology and Paleoanthropology (Beijing, China); **NHMW**, Natural History Museum Wien (Vienna, Austria); **STM**, Shandong Tianyu Museum of Natural History (Pingyi, China); **UWBM**, University of Washington Burke Museum of Natural History and Culture (Seattle, USA).

## RESULTS AND DISCUSSION

### Skeletal Anatomy

In all respects the anatomy of NHMW 1997z0112/0001 is comparable to that of other *Confuciusornis sanctus* specimens (Chiappe et al., 1999). Certain portions of the skeleton preserve morphologies that have not been previously reported, and that as such, are described here using English equivalent of the Latin anatomical nomenclature of Baumel et al. (1993).

**Skull.** The morphology of the skull of NHMW 1997z0112/0001 (Fig. 5) agrees with that described in detail by Chiappe et al. (1999) and largely corroborated by subsequent studies (Elzanowski et al., 2005, 2018). Some of the anatomical details described by Elzanowski et al. (2018) for NHMW 1997z0112/0001 are not validated by the present study. In particular, the description of the postorbital bar as a two-layered structure is problematic, and so is the claim that the jugal, postorbital, quadrate, and zygomatic process are all connected at a point near the ventral end of the postorbital process. In fact, NHMW 1997z0112/0001 clearly shows—corroborating Chiappe et al.'s (1999) description of GMV-2132—that the postorbital bone was caudally connected to a triangular-shaped, ascending process of the jugal (Fig. 5), very much in a typical non-avian theropod fashion. As mentioned by Elzanowski et al. (2018), the postorbital bar of *C. sanctus* is variably

preserved, complicating the interpretation of this region. Nonetheless, there is abundant evidence indicating the full separation of the orbit and the infratemporal fenestra by this bar, and as shown by NHMW 1997z0112/0001, by an ascending process of the jugal that abuts the postorbital bone caudally (Fig. 5). Additionally, the diapsid configuration of the skull of *C. sanctus*, with supratemporal and infratemporal fenestrae separated by a postorbital-squamosal bar (Fig. 5), is also well-documented by the skull of NHMW 1997z0112/0001 (contra Elzanowski et al. (2018)). The jugal-postorbital connection illustrated by NHMW 1997z0112/0001 is congruent with phylogenetic context of *C. sanctus*. Similar cranial configurations are known for more stemward (e.g., *Jeholornis prima*) and more crownward taxa (e.g., Enantiornithes) (Wang et al., 2021) that bracket *C. sanctus* phylogenetically (Fig. 5), and early pygostylians such as the Jinguofortisidae (e.g., *Cratonavis zhui* also retain a diapsid temporal region (Li et al., 2023)). However, the precise homologies of the temporal region of stem birds have yet to be well-understood as the information from available fossils (e.g., lack of a fully enclosed infratemporal fenestra in Archaeopterygidae (Wellnhofer, 2009), partially enclosed supratemporal fenestra of *Ichthyornis dispar* (Field et al., 2018), squamosal that is fully incorporated into the braincase in *Patagopteryx deferrariisi* (Chiappe, 1996, 2002) suggest instances of homoplasy across the basal tree of birds.

**Vertebral Column.** The vertebral column of NHMW 1997z0112/0001 generally agrees with previous descriptions of *Confuciusornis sanctus*. However, the cervical series of this specimen shows clear evidence of the presence of well-developed spinal process (Fig. 6), which were regarded as absent by Chiappe et al. (1999) on the basis of the specimens studied therein. Some of the cervical vertebrae of NHMW 1997z0112/0001 also preserve distinct epiphyses projecting dorsally from the surface of the postzygapophyses (Fig. 6)—these have not been reported for other confuciusornithid taxa (e.g., *Confuciusornis shifan*, *Eoconfuciusornis zhengi*, *Changchengornis hengdaoziensis*, *Yangavis confucii*) (Zhang et al., 2008; Wang & Zhou, 2018; Wang et al., 2022). As described by Chiappe et al. (1999), the morphology of articular facets of the cervical centra is similar to that of enantiornithines, which has been described as having an “incipient heterocoely” (Chiappe, 1996). Namely, while the anterior articular facet is concave laterally and convex dorsoventrally, the posterior articular facet is sub-rounded and only gently concave dorsoventrally. A cervico-thoracic vertebra exposed caudally shows a long spinal process and a vertebral foramen that is larger than the surface of the caudal articular facet (Fig. 6). Published information about the relative size of the vertebral foramen of the pre-sacral vertebrae was previously available for only the thoracic vertebrae, in which this foramen is greatly reduced (Chiappe et al., 1999). A

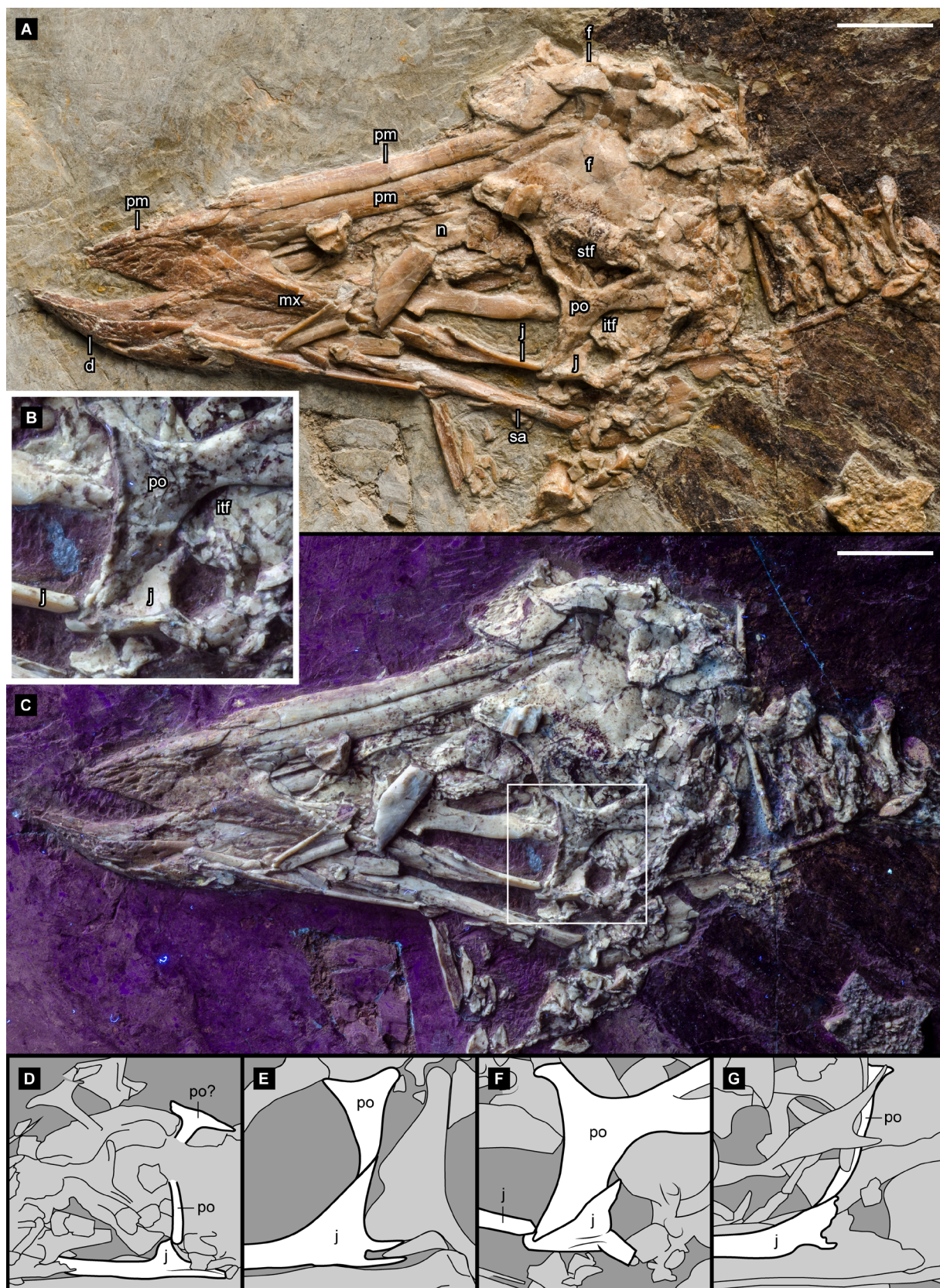


**Figure 5.** A–C, *Confuciusornis sanctus*, NHMW 1997z0112/0001; **A**, skull under normal illumination; **B**, close up of the jugal-postorbital contact under UV light; **C**, skull under UV illumination; **D–G**, comparative drawings of the jugal and postorbital of *Jeholornis prima* (BMNHC-Ph780), *Shenshiornis primita* (LPM-B00018), *Confuciusornis sanctus* (NHMW 1997z0112/0001), and an unnamed enantiornithine (IVPP V12707) in left lateral view (E was flipped horizontally to match D, F, G). *Shenshiornis primita* was regarded as a synonym of *Sapeornis chaoyangensis* by Gao et al. (2012). d, dentary; f, frontal; itf, infratemporal fossa; j, jugal; mx, maxilla; n, nasal; pm, premaxilla; po, postorbital; sa, surangular; stf, supratemporal fossa. D–G not in scale; scale bars (A, C) = 1 cm.



**Figure 6.** A–C, *Confuciusornis sanctus*, NHMW 1997z0112/0001; details of the axial skeleton; **A**, mid-cervical vertebrae; **B**, anterior dorsal vertebrae; **C**, synsacral and caudal vertebrae under UV illumination. **dc**, dorsal crest; **dt**, dorsal trough; **epi**, epiphyses; **il**, ilium; **py**, pygostyle; **sp**, spinal process; **sy**, synsacrum; **vf**, vertebral foramen; **vk**, ventral keel; scale bars = 1 cm.

number of disarticulated thoracic vertebrae are also preserved in NHMW 1997z0112/0001; their anatomy agrees with what was described by Chiappe *et al.* (1999). The synsacrum of NHMW 1997z0112/0001 consists of seven ankylosed vertebrae, as it was described previously for *C. sanctus* and other confuciusornithids (e.g., *Confuciusornis shifan*, *Eoconfuciusornis zhengi*, *Yangavis confucii*) (Zhang *et al.*, 2008; Navalón *et al.*, 2018; Wang *et al.*, 2022). However, NHMW 1997z0112/0001 shows for the first time that the distally expanded transverse processes abutted against the entire length of the ilium. It also shows that towards the caudal end of the synsacrum, these processes angled only slightly, as opposed to in enantiornithines where they are usually strongly angled caudally (Chiappe *et al.*, 1999; Liu *et al.*, 2021). The synsacrum of NHMW 1997z0112/0001 also documents for the first time the presence of a distinct dorsal crest (Fig. 6), representing the co-ossified spinal processes of the synsacral vertebrae, running the entire length of this compound bone. The well-preserved pygostyle of NHMW 1997z0112/0001 (Fig. 6) shows the longitudinal ventral keel and robust laterodorsal ridges defining a deep dorsal trough described by Chiappe *et al.* (1999); its dorsolateral exposure prevents visualization of the proximoventral processes identified by Wang and O'Connor (Wang & O'Connor, 2017).

**Appendicular skeleton.** The forelimb morphology of NHMW 1997z0112/0001 (Fig. 7) agrees in every detail with what was previously described for *Confuciusornis sanctus* (Chiappe *et al.*, 1999). NHMW 1997z0112/0001, a specimen belonging to the largest size class in this species (Marugán-Lobón *et al.*, 2011), confirms that the alular metacarpal (metacarpal I) remained separated (Fig. 7) from the co-ossified major and minor metacarpals (metacarpals II and III) for most (if not all) the life cycle of *C. sanctus*. The well-preserved right wrist of the specimen shows the remarkable size difference between the radiale and the ulnare of *C. sanctus* (Fig. 7)—judging from the reduced size of the ulnare in *Yangavis confucii* (Wang & Zhou, 2018) and *Confuciusornis shifan* (Wang *et al.*, 2022), this condition may be characteristic of all confuciusornithids). NHMW 1997z0112/0001 also shows that the dorsal surface of the alular metacarpal is deeply recessed, developing a deep central fossa proximally.

The morphology of the hindlimb also agrees with previous descriptions (Chiappe *et al.*, 1999). Nonetheless, NHMW 1997z0112/0001 shows that the proximal femur of *C. sanctus* may have had a proximally directed, knob-like posterior trochanter, a condition previously considered unclear or absent (see character codings in Chiappe, 2001; O'Connor *et al.*, 2011; Chiappe *et al.*, 2019). The left tarsometatarsus of NHMW 1997z0112/0001 (Fig. 8) confirms the presence of a metatarsal V in *C. sanctus*. A splint-like element, preserved diagonally on the plantar proximal surface of metatarsal IV, and extending approximately a third of

the metatarsus' length, is visible on the left foot (Fig. 8). While such metatarsal had been reported previously (Hou *et al.*, 1995; Chiappe *et al.*, 1999), it is rarely preserved and it has never been imaged in detail.

**Plumage and soft tissues.** The plumage of NHMW 1997z0112/0001 is preserved in exquisite detail affording precise measurements of the lengths of primary feathers and ornamental rectrices as well as an accurate reconstruction of the wing's length and cord (i.e., wingspan and shape) (Fig. 4; Tab. 1). The wing of this specimen consists of at least 10, and possibly up to 12, primary feathers. This number of primaries falls within the range known for other non-ornithothoracine birds (i.e., long-tailed birds and basal pygostylians) including archaeopterygids (10–12 primaries) (Longrich *et al.*, 2020) and *Sapeornis chaoyangensis* (11–13 primaries) (Gao *et al.*, 2012), and it is greater than what is typical for modern birds (9–10 primaries) (Gill, 2007). The outer primaries are extremely long, being about 3 times the length of the manus. While the extraordinary length of the outer primaries of *Confuciusornis sanctus* has been noticed by previous studies (Wang *et al.*, 2011; Falk *et al.*, 2016; O'Connor, 2020), the apparent number of primaries of NHMW 1997z0112/0001 exceeds the 10 primaries reported by Falk *et al.* (2016) and O'Connor (2020) based on a different specimen (IVPP V13156). The relative lengths of the outer most primaries of NHMW 1997z0112/0001 are largely consistent with what was reported for IVPP V13156 (Falk *et al.*, 2016). In NHMW 1997z0112/0001, the outermost primary (P12) is approximately half the length of the penultimate primary (P11), and P8 (roughly as long as P10 and P9) is the longest feather (Fig. 9). These proportions agree with what was described by Falk *et al.* (2016) and O'Connor (2020) for IVPP V13156; however, P11–7 are much closer in length than what was reported by O'Connor (2020), who indicated that the third through fifth primaries (corresponding to P10–P8 in NHMW 1997z0112/0001) were 20–25% longer than the penultimate primary (corresponding to P11 in NHMW 1997z0112/0001). The spread-out preservation of P11–P7 on both wings of NHMW 1997z0112/0001 (Fig. 9), leaves no doubt about the relative proportions of the five longest primaries. Measurements of the width of the rachises are far less certain, as it has been highlighted previously for other specimens of *C. sanctus* (Zheng *et al.*, 2010). Our estimates of these measurements suggest an approximate width of 1.5 mm for the rachises of the middle portion of the outer primaries and a 0.70–0.60 mm range for the distal portion of these feathers (Fig. 1). These estimates fall in between to those provided by Nudds and Dyke (2010) and Zheng *et al.* (2010). We concur with these authors that the rachises of *C. sanctus* are generally thinner than those of living birds of similar body mass but caution about making inferences on their mechanical attributes based on comparisons to modern birds given recent data showing how the developmental and

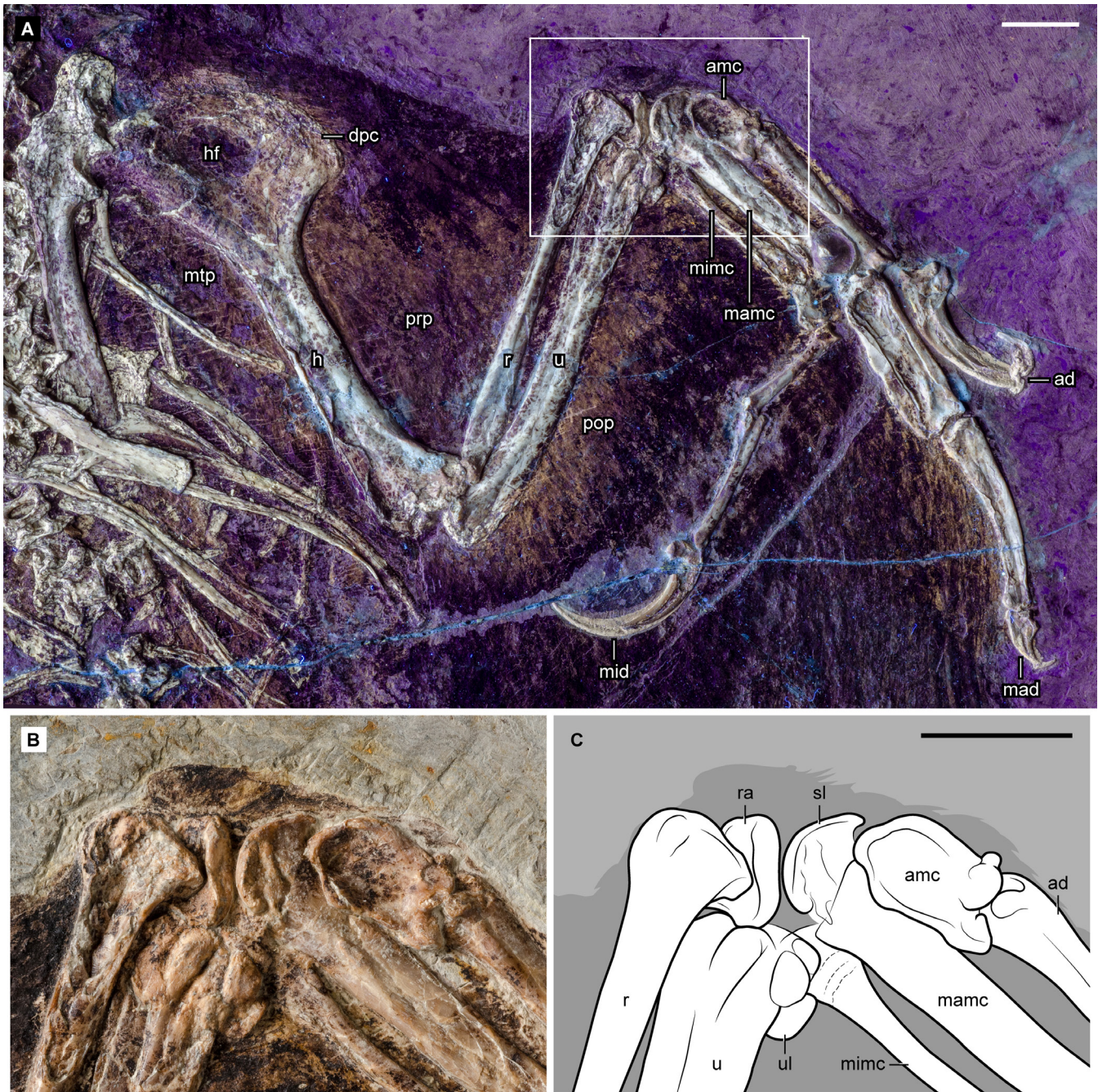


**Figure 7. A–C, *Confuciusornis sanctus*, NHMW 1997z0112/0001; A, right forelimb under UV illumination; B, detail of the wrist (box in A) under normal illumination; C, interpretive drawing of B. Note the preservation of soft tissue corresponding to the three patagia of the wing (metapatagium, postpatagium, and propatagium) in A. ad, alular digit; amc, alular metacarpal; dpc, deltopectoral crest; h, humerus; hf, humeral foramen; mad, major digit; mamc, major metacarpal; mid, minor digit; mimc, minor metacarpal; mtp, metapatagium; pop, postpatagium; prp, propatagium; r, radius; ra, radiale; sl, semilunar carpal; u, ulna; ul, ulnare; scale bars = 1 cm.**

mechanical aspects of the feathers of stem birds need not to be similar to those of their living counterparts (Carroll et al., 2019).

The rectrices surrounding the pygostyle lack a pennaceous arrangement (sometimes described as ‘rachis-less’ or ‘non-shafted’) (Fig. 9), as it has been observed for other specimens of *Confuciusornis sanctus* (Wang & O’Connor, 2017). The long (left: 286 mm; right: 295.5 mm) pair of rachis-dominated feathers (RDFs) define an angle of approximately

9.5°, and their bases converge towards the pygostyle and its surrounding rectrices (Fig. 10). Like all other RDFs, these feathers consist of a rather stiff, uniformly broad rachis, with a dark, longitudinal median stripe. Transversally (*i.e.*, medial to lateral margin, and vice versa) and throughout most of their length (except for the vaned distal portion), these feathers show a distinct pattern of color: dark-brown longitudinal bands (running both laterally and medially) bracket a central, lighter portion that contains the thin median stripe (Fig. 10).



**Figure 8. A–B**, *Confuciusornis sanctus*, NHMW 1997z0112/0001; **A**, left foot in plantar view; **B**, detail of the proximal half of the tarsometatarsus (box in A). **I–IV**, pedal digits I–IV; **mt I–V**, metatarsals I–V; scale bars = 1 cm (A) and 0.5 cm (B).

Three-dimensional RDF inclusions in mid-Cretaceous amber from Myanmar have demonstrated that the median stripe corresponds to a dorsal groove/ventral ridge that runs along the length of the feathers (Xing et al., 2018; Carroll et al., 2019). The dark-brown bands on either side of the RDFs of NHMW 1997z0112/0001 narrow distally as the central, lighter band becomes broader (the width of the feather remains somewhat uniform) (Fig. 10). However, NHMW 1997z0112/0001 clearly shows that as the dark-brown bands taper distally, the lateral band of each feather is thicker (Fig. 10). Most likely, these distinctly toned components of the RDFs represent distinct structural constituents (like in the case of the median stripe) and perhaps, they could have been characterized by differential coloration. Foth (2020) suggested that the dark lateral

margins of these feathers could either correspond to highly pigmented cortical ridges or to a preservation artifact caused by the preservation of short, packed, and highly pigmented barbs that cannot be differentiated through normal light microscopy—the latter, however, seems unlikely in light of the evidence derived from three-dimensional inclusions in amber (Xing et al., 2018; Carroll et al., 2019). The specific significance of these color patterning is still at large but future studies of amber inclusions or geochemical analyses on the feathers (e.g., Raman spectroscopy) may provide a better understanding of the structure of these feathers. Individualized barbs are absent throughout most of the length of these feathers. However, at the beginning of the distal fifth of these feathers, the lighter band starts to taper more acutely as densely packed barbs (preserved



**Figure 9.** A–B, *Confuciusornis sanctus*, NHMW 1997z0112/0001; **A**, detail of distal primaries and partial RDF rectrices (rachis dominated feathers); **B**, detail of left primaries; **C**, detail of ‘rachis-less’ rectrices. **fe**, femur; **P7–11**, primaries 7–11; **py**, pygostyle; **RDF**, rachis-dominated feathers; **rlr**, rachis-less rectrices; **sy**, synsacrum. White arrows in B point at the rachises of the left primaries; scale bars = 1 cm (A, C) and 0.5 cm (B).



**Figure 10.** A–E, *Confuciusornis sanctus*, NHMW 1997z0112/0001; A–C, details of the right rachis dominated feather (RDF) as indicated in D–E, full length (D) and interpretive drawing (E) of RDFs. Note the distinct median stripe, and the transition between a proximocentral zone characterized by an externally thick and dark band containing a thin lighter band (A) to distal zone characterized by an externally thin and dark band containing a thick lighter band (C). **mes**, median stripe; **vap**, vaned portion; scale bars = 0.5 cm (A–C) and 1 cm (D–E).

as dark-brown) gradually develop symmetrical vanes on either side (Fig. 10). The lack of differentiated vanes in RDFs has been confirmed by studies of inclusions in amber (Xing et al., 2018; Carroll et al., 2019), which have also demonstrated the lack of medullary pith and caution developmental interpretation of these feathers in the context of modern feather development (contra Foth (2020)). The lighter band disappears within 15 mm from the above-mentioned onset of sharp tapering. In NHMW 1997z0112/0001—as well as in some other specimens of *C. sanctus* (Chiappe et al., 1999)—the width of the two vanes is equivalent (7.1 mm at the left feather's widest point); this appears not to be the case in all specimens of *C. sanctus*, where the medial vane seems to be slightly wider (O'Connor, 2020).

Some general preservation of other soft tissues is visualized through UV illumination. While soft tissues are preserved outlining the fleshy portions of the specimen (e.g., torso, thigh, and shin), the best preserved of these correspond to remnants of the wing patagia (i.e., proapatagium, postapatagium, and metapatagium) (Fig. 7). The morphology of these patagia is comparable to what was reported by Falk et al. (2016). The combination of soft tissues and plumage around the shin corroborates previous claims (Chiappe & Meng, 2016; O'Connor, 2020) contradicting the report of elongated crural and tarsal feathers in *C. sanctus* (Zheng et al., 2013).

### Flight reconstruction of *Confuciusornis sanctus*

Abundant anatomical evidence (e.g., well-developed sternum and shoulder muscles, expanded proximal humerus, shape of wing feathers, and presence of patagia) suggests that *Confuciusornis sanctus* and other confuciusornithids were capable of some kind of powered flight (Chiappe et al., 1999; Rayner, 2001; Zheng et al., 2013; Falk et al., 2016; Wang et al., 2022; Pittman et al., 2022). The exceptional preservation of the skeleton and feathers of NHMW 1997z0112/0001 provide the basis for inferences on the aerial competence of this bird. Using the multiple regressions approach (MR), we estimated that NHMW 1997z0112/0001 had a body mass of 0.615 kg (range 0.511–0.719 Kg), a wing span of 0.862 m (0.839–0.884 m), and a wing area of 0.112 m<sup>2</sup> (0.104–0.120 m<sup>2</sup>) (Tab. 2). Values obtained from the outline reconstructions (OR) of the spread wing varied just 2% of those derived from multiple regressions for wingspan (0.881 m vs 0.862 m), but 10–25% for the wing area (0.084–0.101 m<sup>2</sup> vs 0.112 m<sup>2</sup>). Such a notable difference in the estimations of wing area is likely due to the fact that the OR approach considers the exceptional length of the outermost primaries, which results in a marked 'step' in the trailing-edge of the distal wing (Fig. 3). This differential length of the outermost primaries, when compared to the remaining primaries and secondaries, is observed in numerous specimens of *C. sanctus* (pers. obs.), and consequently it is unlikely to represent a molting pattern

of wing feathers in NHMW 1997z0112/0001. Instead, it could be an analogue of the trailing-edge notch present in the wings of land fowl and sandgrouse. For this reason, we regard the OR estimations of the wing area to be more accurate than the one obtained from the MR approach. Drovetski (1996) demonstrated that the wing design of land fowl and sandgrouse—with the above-mentioned trailing-edge notch—reduces the efficiency of level (i.e., flapping) flight while it increases the lift-to-drag ratio that benefits slow flight.

The values of wing aspect ratio and relative wing loading calculated for NHMW 1997z0112/0001 using the OR approach were 7.7–9.3 and 6.3–9.8 Kg/m<sup>2</sup>, respectively (Tab. 2). Such combination matches that of distantly related, small and medium-sized birds that fly through sustained flapping (i.e., *Syrnhaptes paradoxus*, *Tringa nebularia*, *Charadrius hiaticula*, *Calidris alpina*, *Tadorna tadorna*) and also through flap-gliding (i.e., *Falco peregrinus*, *Delichon urbica*) (Fig. 11). The wing of Palla's Sandgrouse, *S. paradoxus*, is an example of the above-mentioned trailing-edge notch (see detail in Fig. 11). The aspect ratio and wing loading values obtained from the MR approach—an aspect ratio of 6.5–6.7 and a wing loading of 5.5 Kg/m<sup>2</sup> (4.9–6.0 Kg/m<sup>2</sup>)—were lower than those obtained from the reconstructed wing. In this case, NHMW 1997z0112/0001 matched better the values for small-to-medium sized birds that fly through different strategies, including sustained flapping (e.g., *Columba rupestris*, *Pluvialis squatarola*), bounding (e.g., *Motacilla flava*), flap-gliding (e.g., *Artamus personatus*), and some short-time fliers (e.g., *Gallinix cinerea*) (Fig. 11).

In modern birds, active flapping is constrained by the ratio between the power available from aerobic metabolism ( $P_{av}$ ) and the mechanical power output required for flapping ( $P_{mec}$ ) (Rayner, 1988; Norberg, 2002; Pennycuik, 2008). By assuming a negative scaling between  $P_{av}$  and body mass, as observed in extant flying birds (Bishop & Butler, 1995, 2015), and a conversion efficiency of 0.2 between total metabolism and  $P_{av}$  (Tucker, 1973; Pennycuik, 2008), NHMW 1997z0112/0001 would have had 5.4–6.9 W of available power ( $P_{av}$ ) for continuous flapping (with muscles working aerobically). Compared to the values of  $P_{mec}$  calculated from the MR approach (i.e., 6.5 to 10.6 W at minimum power speed) (Fig. 12; Tab. 2),  $P_{av}$  would have been insufficient to cover the energetic requirements for flapping flight for most of the range of forward speeds. However, when using the OR approaches, the power margin between the ranges of  $P_{av}$  and  $P_{mec}$  raises the possibility that NHMW 1997z0112/0001 could have flown using continuous flapping (under aerobic conditions) at speeds between 9 to 16 m/s (Fig. 12). It is noteworthy that a considerable range of uncertainty for speeds in the models (OR1-3 and MR) show a negative power margin (i.e.,  $P_{av} < P_{mec}$ ; Fig. 12), which indicates that the aerobic activity of the flight muscles was insufficient for sustained flapping flight. Such an energetic limitation, together with the

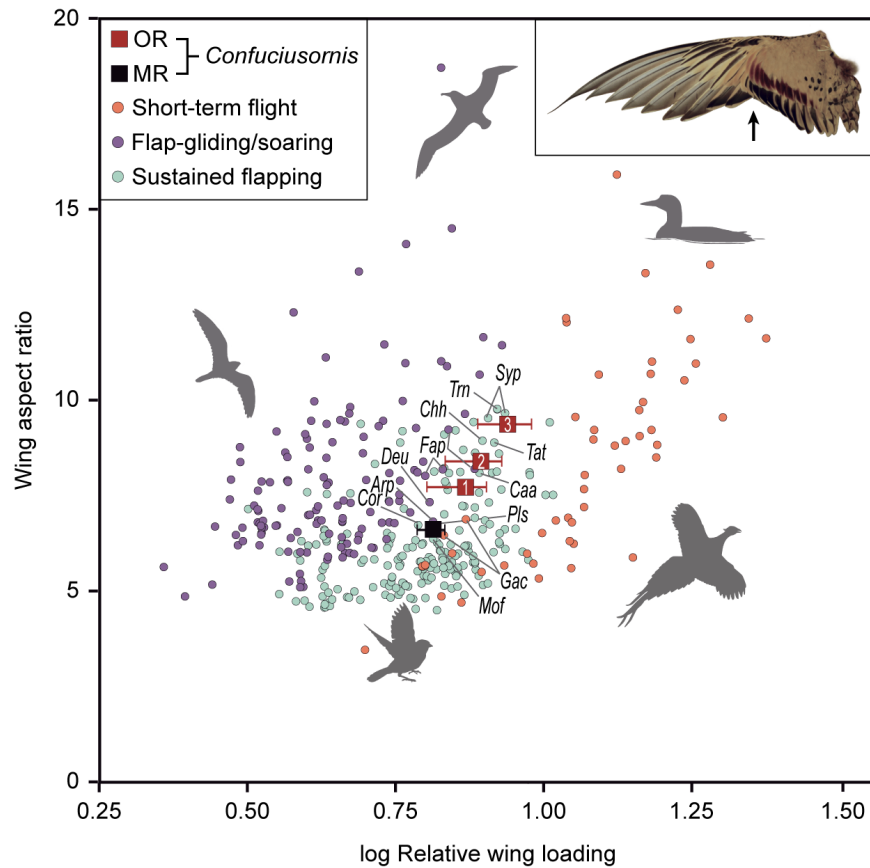


**Figure 11.** Scatter diagram of aspect ratio (*AR*) on relative wing loading (*RWL*). Colored dots represent three main strategies used by modern flighted birds. Squares indicate the position of NHMW 1997z0112/0001 in the morphospace according the two approaches (the size of the bar represents *RWL* uncertainty estimates): outline reconstructions (OR1, OR2 and OR3) in red, and multiple regression (MR) in black. The spread wing of the Pallas’s Sandgrouse, *Syrrhaptes paradoxus*, is shown in the top right of the graph with an arrow indicating the trailing-edge notch. Abbreviations: **Arp**, *Artamus personatus*; **Caa**, *Calidris alpina*; **Chh**, *Charadrius hiaticula*; **Cor**, *Columba rupestris*; **Deu**, *Delichon urbica*; **Fap**, *Falco peregrinus*; **Gac**, *Gallixrex cinerea*; **Mof**, *Motacilla flava*; **Pls**, *Pluvialis squatarola*; **Syp**, *Syrrhaptes paradoxus*; **Tat**, *Tadorna tadorna*; **Trn**, *Tringa nebularia*.

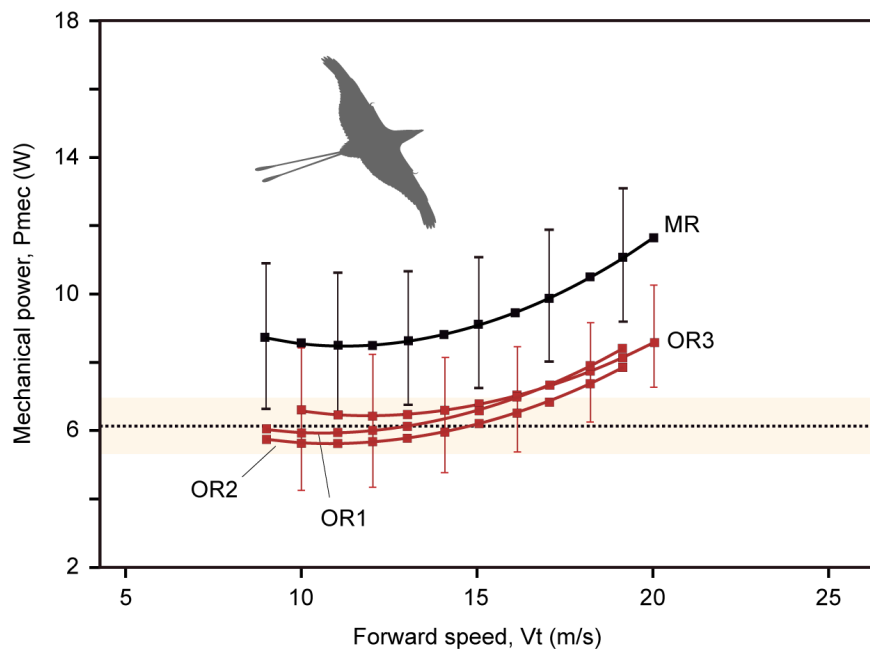


**Figure 12.** Energetic fitness of *Confuciusornis* NHMW 1997z0112/0001 for maintaining flapping flight as depicted by the power margin ( $P_{av}/P_{mec}$ ). Estimations for the maximum aerobic power available ( $P_{av}$ ; horizontal dashed line) and the mechanical power output for flapping flight ( $P_{mec}$ ; black and red lines) include uncertainty ranges (obtained from the lowest and highest estimations of body mass, wing span, and wing area) depicted as a horizontal orange band and vertical error bars, respectively.

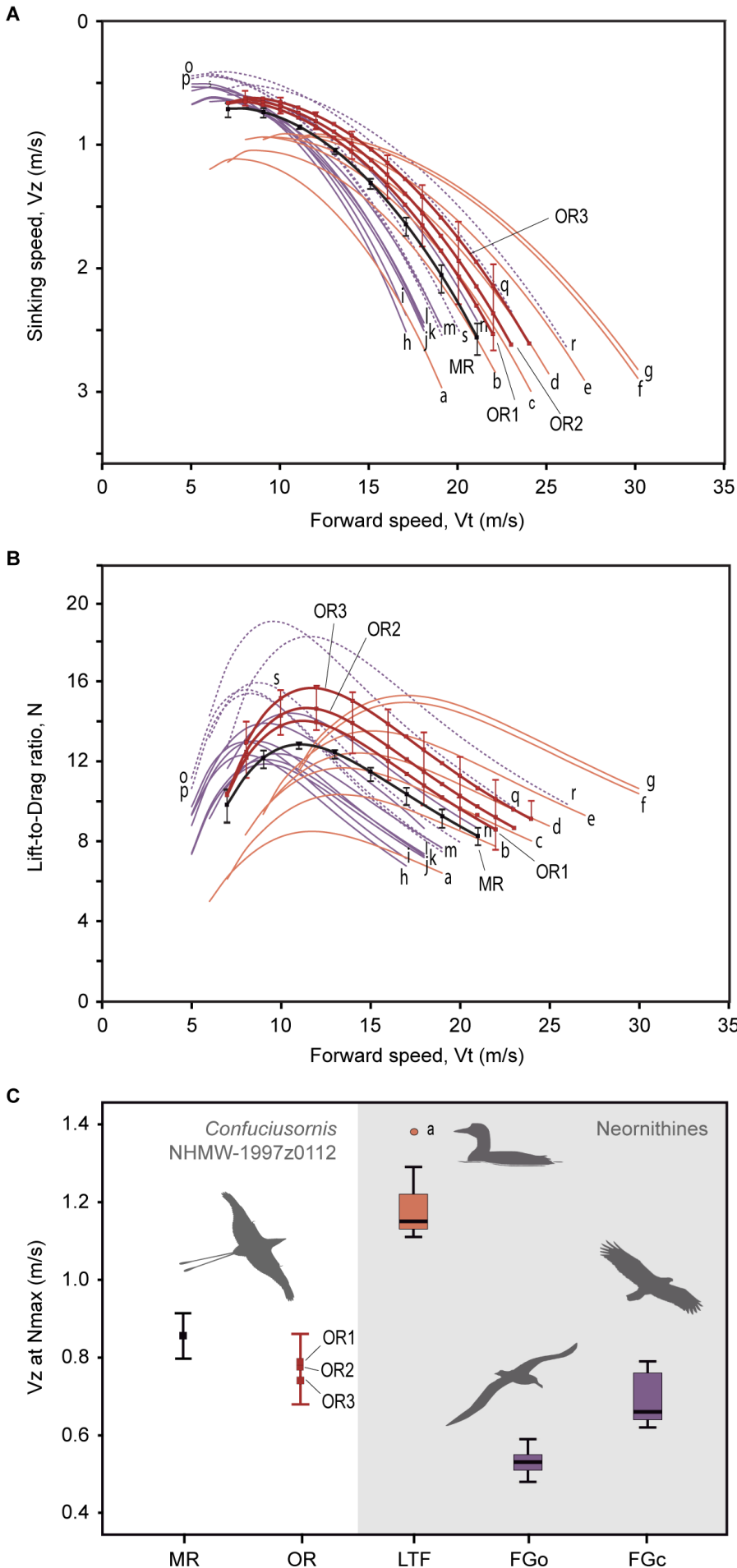


**Figure 13.** Gliding fitness of *Confuciusornis* NHMW 1997z0112/0001 compared to similarly-sized extant birds. **A**, Gliding pattern as depicted by the relationship between forward ( $V_t$ ) and sinking speed ( $V_z$ ). Selected extant birds are classified on the basis of whether they usually fly through oceanic soaring-gliding (purple dashed lines), continental soaring-gliding (purple solid lines), or whether they use flight as a secondary way of locomotion (orange lines) (Tab. 3); **B**, aerodynamic fitness as depicted by the variation of the lift-to-drag ratio (N) with the forward speed ( $V_t$ ); **C**, range for the best gliding speed. Box length shows the interquartile range (25<sup>th</sup> and 75<sup>th</sup> percentiles), and whisker lengths indicate the 5–95% confidence limits. Middle thick line represents the median value. For NHMW 1997z0112/0001, whiskers represent the uncertainty from the estimation errors. ANOVA and post-hoc tests indicate significant differences between all groups ( $p < 0.01$ ) (Tab. 4). Selected modern birds: a-*Centropus milo*; b-*Megapodius freycinet*; c-*Porphyrio porphyrio*; d-*Lagopus lagopus*; e-*Fulica atra*; f-*Uria aalge*; g-*Podiceps cristatus*; h-*Bubo virginianus*; i-*Hieraaetus pennatus*; j-*Corvus corone*; k-*Circus aeruginosus*; l-*Ninox novaeseelandiae*; m-*Accipiter gentilis*; n-*Falco peregrinus*; o-*Larus argentatus*; p-*Stercorarius pomarinus*; q-*Puffinus diomedea*; r-*Fulmarus glacialis*; s-*Larus fuscus*.

**Table 4.** Results of Bonferroni's post-hoc test comparing differences in sink at maximum lift-to-drag ratio (*i.e.*,  $V_z$  at  $N_{max}$ ) between either, the groups of modern flight strategies (**FGc**, continental soaring birds; **FGo**, oceanic soaring birds; **LTF**, short-time fliers) and the grouping values reconstructed for *Confuciusornis* from MR, OR1, OR2 and OR3.

		Difference between means	Standard error	p-value
FGc	FGo	0.161	0.042	< 0.01
	LTF	-0.498	0.038	< 0.001
	<i>Confuciusornis</i>	-0.098	0.033	0.036
FGo	FGc	-0.161	0.042	< 0.01
	LTF	-0.659	0.044	< 0.001
	<i>Confuciusornis</i>	-0.259	0.040	< 0.001
LTF	FGc	0.498	0.038	< 0.001
	FGo	0.659	0.044	< 0.001
	<i>Confuciusornis</i>	0.401	0.035	< 0.001

mechanical limitation for modern-like flapping imposed by the scapulocoracoid fusion and glenoid orientation of *Confuciusornis sanctus* (Senter, 2006; Wu et al., 2021), makes unlikely that NHMW 1997z0112/0001 could have performed prolonged flights using only sustained flapping. That said, given that modern birds can use gliding to extend flight duration and reduce energetic costs with respect to continuous flapping (Muijres et al., 2012; Sachs, 2015), these energetic and anatomical limitations do not rule out the capacity of *Confuciusornis sanctus* for performing prolonged flights (based on NHMW 1997z0112/0001). In fact, our aerodynamic reconstruction of NHMW 1997z0112/0001 shows a gliding pattern closer to that of birds that usually soar and glide using continental air currents, and it is conceivable that this specimen could have been able to glide at low speeds with relatively low lift-to-drag ratios (Fig. 13A–13B). Data on modern fliers show that when birds glide at their maximum performance (*i.e.*, best glide speed, when the ratio between forward speed to sink is at its maximum), values for sinking speed differ significantly between short-time fliers (*e.g.*, land fowl and rails), continental soaring birds (*e.g.*, raptors and crows), and oceanic soaring birds (*e.g.*, seabirds) (Tab. 4; Fig. 13C). Our results indicate that when NHMW 1997z0112/0001 reached its maximum lift-to-drag ratio (12.7–13.0 according to the MR model, and 14.1–15.7 in the OR models), its gliding forward velocity ranged from 10.2 to 12.9 m/s, and its sinking speed from 0.7 to 0.9 m/s. While these values are slightly higher than those of modern gliding birds (low significant difference from continental soarers), they demonstrate that the gliding capabilities of NHMW 1997z0112/0001 would have been notably higher than those of extant short-time fliers, as its sinking speed would have been significantly slower than those for these birds when they glide at maximum gliding speed (Tab. 4; Fig. 13C). Some studies have claimed that *Confuciusornis sanctus* was unable to achieve prolonged flights (Nudds & Dyke, 2010; Falk et al., 2016). However,

our results support that *C. sanctus* could be able to perform prolonged flight as long as this bird alternated periods of active flapping supported by muscles with periods of efficient low-speed gliding. The duration of the active period would have been longer in case of higher power margin to muscles work aerobically (*i.e.*, models OR1 and OR2 between 9–15 m/s) compared to muscles working anaerobically (*i.e.*, model MR) (Fig. 2). It is noteworthy that our OR reconstructions also raises the possibility of aerobically sustained flapping while flying between 9 and 16 m/s (Fig. 12) and gliding with the maximum lift-to-drag ratio (Fig. 13B). The combination of flapping and gliding at these forward speeds supports the hypothesis that *C. sanctus* could have conducted energetically-efficient, prolonged flights. This implies a potential capacity for ecological dispersal (*e.g.*, seasonal migration, movement from birth site to breeding site, movement between different breeding sites). The dominance of gliding periods within a full-cycle of flap-gliding flight is consistent with the enlarged proximal epiphysis of the humerus (Serrano & Chiappe 2017), and would have mitigated limitations for a modern-like wing stroke (Wu et al., 2021) and reduced stress on the flight feathers of *C. sanctus*, whose vane configuration points at a low capacity for maintaining a coherent airfoil during downstroke (Feo et al., 2015).

## CONCLUSION

NHMW 1997z0112/0001 is among the best-preserved specimens of *Confuciusornis sanctus*, and its morphology affords osteological information previously unreported in the literature, particularly from the cervical and synsacral regions of the axial skeleton, and the appendicular skeleton. Most notably, the plumage of this specimen provides precise measurements of the remiges and rectrices, and information needed for an accurate reconstruction of the wing shape of this species. Multiple regression analyses of the skeletal measurements of NHMW 1997z0112/0001 estimate a body mass ( $M_B$ ) of approximately 615 grams, roughly equivalent to the size of a Carrion Crow (*Corvus corone*) and falling within the largest size class reported for *C. sanctus* by Marugán-Lobón et al. (2011). Our estimation of the wing shape of NHMW 1997z0112/0001 points at a wingspan ( $B$ ) of 83.9–88.4 cm and a lift surface ( $S_L$ ) of 840–1120 cm<sup>2</sup>. The accuracy of these estimations is corroborated by values derived from the outline reconstructions (OR) of the wing and from multiple regression (MR) analyses. Evidence from these estimations, the wing loading and aspect ratio of NHMW 1997z0112/0001, and the aerodynamic modeling, provide strong support against previous claims indicating that the flight capabilities of *C. sanctus* were at best limited to short flights. In contrast, our results support that *C. sanctus* would have been capable of undertaking prolonged flights as long as it alternated periods of high-efficiency gliding

with active flapping; the duration of this active period would have been longer in case of higher power margin from aerobic muscle activity, which varied with  $V_f$  and the model analyzed (e.g., OR1 > MR, Fig. 12).

Together with recent evidence indicating soaring specializations among other basal pygostylians (*i.e.*, *Sapeornis chaoyangensis*) (Serrano & Chiappe, 2017), and potential for bounding (Serrano *et al.*, 2018) and flap-gliding flight (Chiappe *et al.*, 2019) in enantiornithines, our results highlight how birds developed energy-savings strategies to improve aerial efficiency very early in their evolutionary history.

**Supplementary information.** This article has no additional data.

**Author contributions.** All authors participated in the design of the experiments and wrote various portions of the manuscript.

**Competing interest.** We declare no competing interests.

**Funding.** Main research funding was provided by the Dinosaur Institute of the Natural History Museum of Los Angeles County. FJS received funding from the Spanish Ministry of Science and Innovation (Research Project PID2019-111185GB and Juan de la Cierva-Incorporación Fellowship IJCI-2017-32116), and the Junta de Andalucía (PAIDI grant 2020-00095).

**Author details.** Luis M. Chiappe<sup>1</sup>, Francisco J. Serrano<sup>1,2</sup>, Stephanie Abramowicz<sup>1</sup>, & Ursula B. Göhlich<sup>3</sup>. <sup>1</sup>Dinosaur Institute, Natural History Museum of Los Angeles County, 900 Exposition Boulevard, CA 90007 Los Angeles, USA; lchiappe@nhm.org, sabramow@nh.org; <sup>2</sup>Universidad de Málaga, Campus de Teatinos s/n, 29071 Málaga, Spain; fjsa@uma.es; <sup>3</sup>Naturhistorisches Museum Wien, 3. Zoologische Abteilung, Bruggrind 7, 1010 Vienna, Austria; ursula.goehlich@nhm-wien.ac.at

**Acknowledgements.** We are grateful to Franz Topka (Naturhistorisches Museum Wien), who painstakingly prepared the specimen. We also thank to Colin Palmer, Jesús Marugán-Lobón and an anonymous reviewer for their insightful comments that improved earlier versions of this article.

## REFERENCES

- Baumel, J. J., King, K. S., Breazile, J. E., Evans, H. E., & Berge, J. C. V. (1993). *Handbook of Avian Anatomy: Nomina Anatomica Avium*. Nuttall Ornithological Club.
- Bishop, C. M., & Butler, P. J. (1995). Physiological modeling of oxygen consumption in birds during flight. *Journal of Experimental Biology*, 198, 2153–2163. doi: [10.1242/jeb.198.10.2153](https://doi.org/10.1242/jeb.198.10.2153)
- Bishop, C. M., & Butler, P. J. (2015). Flight. In C. G. Scanes (Ed.), *Sturkie's Avian Physiology* (pp. 919–974). Academic Press.
- Carroll, N. R., Chiappe, L. M., & Bottjer, D. J. (2019). Mid-Cretaceous amber inclusions reveal morphogenesis of extinct rachis-dominated feathers. *Scientific Reports*, 9, 18108. doi: [10.1038/s41598-019-54429-y](https://doi.org/10.1038/s41598-019-54429-y)
- Chiappe, L. M. (1996). Late Cretaceous birds of southern South America: anatomy and systematics of Enantiornithes and *Patagopteryx deferrariisi*. *Münchner Geowissenschaftliche Abhandlungen (A)*, 30, 203–244.
- Chiappe, L. M., Ji, S., Ji, Q., & Norell, M. A. (1999). Anatomy and systematics of the Confuciusornithidae (Theropoda: Aves) from the late Mesozoic of northeastern China. *Bulletin of the American Museum of Natural History*, 242, 1–89.
- Chiappe, L. M. (2001). Phylogenetic relationships among basal birds. In J. Gauthier, & L. F. Gall (Eds.), *New perspectives on the origin and early evolution of birds: proceedings of the international symposium in honor of John H. Ostrom* (pp. 125–139). Peabody Museum of Natural History, Yale University.
- Chiappe, L. M. (2002). Osteology of the flightless *Patagopteryx deferrariisi* from the Late Cretaceous of Patagonia (Argentina). In L. M. Chiappe, & L. M. Witmer (Eds.), *Mesozoic Birds: Above the heads of dinosaurs* (pp. 281–316). University of California Press.
- Chiappe, L. M., Marugán-Lobón, J., Ji, S., & Zhou, Z. (2008). Life-History of a basal bird: morphometrics of the Early Cretaceous *Confuciusornis*. *Biology Letters*, 4, 719–723. doi: [10.1098/rsbl.2008.0409](https://doi.org/10.1098/rsbl.2008.0409)
- Chiappe, L. M., & Meng, Q. (2016). *Birds of Stone: Chinese Avian Fossils from the Age of Dinosaurs*. John Hopkins University Press.
- Chiappe, L. M., Meng, Q., Serrano, F., Sigurdson, T., Wang, M., Bell, A., & Liu, D. (2019). New *Bohaiornis*-like bird from the Early Cretaceous of China: enantiornithine interrelationships and flight performance. *PeerJ*, 7, e7846. doi: [10.7717/peerj.7846](https://doi.org/10.7717/peerj.7846)
- Chinsamy A., Chiappe L. M., Marugán-Lobón J., Gao, C., & Zhang, F. (2013). Gender identification of the Mesozoic bird *Confuciusornis sanctus*. *Nature Communications*, 4, 1381. doi: [10.1038/ncomms2377](https://doi.org/10.1038/ncomms2377)
- Chinsamy, A., Marugán-Lobón, J., Serrano, F. J., & Chiappe, L. M. (2020). Life History of the basal pygostylian, *Confuciusornis sanctus* as deduced by osteohistology. *Anatomical Records*, 303, 949–962. doi: [10.1002/ar.24282](https://doi.org/10.1002/ar.24282)
- Dalsätt, J., Zhou, Z., Zhang, F., & Ericson, P. G. P. (2006). Food remains in *Confuciusornis sanctus* suggest a fish diet. *Naturwissenschaften*, 93, 444–446. doi: [10.1007/s00114-006-0125-y](https://doi.org/10.1007/s00114-006-0125-y)
- Drovetski, S. V. (1996). Influence of the trailing-edge notch on flight performance of galliforms. *Auk*, 113, 802–810.
- Elzanowski, A. J., Manegold, A., & Peters, D. S. (2005). Redescription of a skull of *Confuciusornis sanctus*. *Archaeopteryx*, 23, 51–55.
- Elzanowski, A. J., Peters, D. S., & Mayr, G. (2018). Cranial morphology of the Early Cretaceous bird *Confuciusornis*. *Journal of Vertebrate Paleontology*, 38, 2, doi: [10.1080/02724634.2018.1439832](https://doi.org/10.1080/02724634.2018.1439832)
- Falk, A., Kaye, T. G., Zhou, Z., & Burnham, D. A. (2016). Laser fluorescence illuminates the soft tissue and life habits of the Early Cretaceous bird *Confuciusornis*. *PLoS One*, 11, e0167284. doi: [10.1371/journal.pone.0167284](https://doi.org/10.1371/journal.pone.0167284)
- Falk, A., O'Connor, J., Wang, M., & Zhou, Z. (2019). On the preservation of the beak in *Confuciusornis* (Aves: Pygostylia). *Diversity*, 11, 212. doi: [10.3390/d11110212](https://doi.org/10.3390/d11110212)
- Feo, T., Field, D. J., & Prum, R. O. (2015). Barb geometry of asymmetrical feathers reveals a transitional morphology in the evolution of avian flight. *Proceedings of the Royal Society B*, 282, 20142864. doi: [10.1098/rspb.2014.2864](https://doi.org/10.1098/rspb.2014.2864)
- Field, D. J., Hanson, M., Burnham, D., Wilson, L. E., Super, K., Ehret, D., Ebersoles, J., & Bhullar, B.-A. (2018). Complete *Ichthyornis* skull illuminates mosaic assembly

- of the avian head. *Nature*, 557, 96–100. doi: [10.1038/s41586-018-0053-y](https://doi.org/10.1038/s41586-018-0053-y)
- Foth, C. (2020). A morphological review of the enigmatic elongated tail feathers of stem birds. In C. Foth, & O. W. M. Rauhut (Eds.), *The evolution of feathers: from the origin to the present* (pp. 173–184). Springer Nature.
- Gao, C., Chiappe, L. M., Zhang, F., Pomeroy, D., Shen, C., Chinsamy, A., & Walsh, M. O. (2012). A subadult specimen of the Early Cretaceous bird *Sapeornis chaoyangensis* and a taxonomic reassessment of sapeornithids. *Journal of Vertebrate Paleontology*, 32, 1103–1112. doi: [10.1080/02724634.2012.693865](https://doi.org/10.1080/02724634.2012.693865)
- Gill, F. B. (2007). *Ornithology*. W. H. Freeman & Co.
- Hou, L., Zhou, Z., Gu, Y., & Zhang, H. (1995). *Confuciusornis sanctus*, a new Late Jurassic sauriurine bird from China. *Chinese Science Bulletin*, 40, 1545–1551.
- Hou, L., Martin, L. D., Zhou, Z., Feduccia, A., & Zhang, F. (1999). A diapsid skull in a new species of the primitive bird *Confuciusornis*. *Nature*, 399, 679–682. doi: [10.1038/21411](https://doi.org/10.1038/21411)
- Li, Q., Clarke, J. A., Gao, K., Peteya, J., & Shawkey, M. (2018). Elaborate plumage patterning in a Cretaceous bird. *PeerJ*, 6, e5831. doi: [10.7717/peerj.5831](https://doi.org/10.7717/peerj.5831)
- Li, Z., Wang, M., Stidham, T. A., & Zhou, Z. (2023). Decoupling the skull and skeleton in a Cretaceous bird with unique appendicular morphologies. *Nature Ecology & Evolution*, 7, 20–31. doi: [10.1038/s41559-022-01921-w](https://doi.org/10.1038/s41559-022-01921-w)
- Liu, D., Chiappe, L. M., Wu, H., Meng, Q., Zhang, Y., Qiu, R., Xing, H., & Zeng, Z. (2021). Cranial and dental morphology in a bohaiornithids enantiornithine with information on its tooth replacement pattern. *Cretaceous Research*, 129, 105021. doi: [10.1016/j.cretres.2021.105021](https://doi.org/10.1016/j.cretres.2021.105021)
- Longrich, N. R., Tischlinger, H., & Foth, C. (2020). The feathers of the Jurassic Urvogel *Archaeopteryx*. In C. Foth, & O. W. M. Rauhut (Eds.), *The evolution of feathers: from the origin to the present* (pp. 119–146). Springer Nature.
- Martin, L. D., Zhou, Z. H., Hou, L. H., & Feduccia, A. (1998). *Confuciusornis sanctus* compared to *Archaeopteryx lithographica*. *Naturwissenschaften*, 85, 286–289. doi: [10.1007/s001140050501](https://doi.org/10.1007/s001140050501)
- Marugán-Lobón J., Chiappe, L. M., Ji, S., Zhou, Z., Gao, C., Hu, D., & Meng Q. (2011). Quantitative patterns of morphological variation in the appendicular skeleton of the Early Cretaceous bird *Confuciusornis*. *Journal of Systematic Palaeontology*, 9, 91–101. doi: [10.1080/14772019.2010.517786](https://doi.org/10.1080/14772019.2010.517786)
- Marugán-Lobón J., & Chiappe, L. M. (2022). Ontogenetic niche shifts in the Mesozoic bird *Confuciusornis sanctus*. *Current Biology*, 32, 1629–1634. doi: [10.1016/j.cub.2022.02.010](https://doi.org/10.1016/j.cub.2022.02.010)
- Muijres, F. T., Henningson, P., Stuijver, M., & Hedenstrom, A. (2012). Aerodynamic flight performance in flap-gliding birds and bats. *Journal of Theoretical Biology*, 306, 120–128. doi: [10.1016/j.jtbi.2012.04.014](https://doi.org/10.1016/j.jtbi.2012.04.014)
- Navalón, G., Meng, Q., Marugán-Lobón, J., Zhang, Y., Wang, B., Xing, H., Liu, D., & Chiappe, L. M. (2018). Diversity and evolution of the *Confuciusornithidae*: evidence from a new 131-million-year-old specimen from the Huajiyi Formation in northeastern China. *Journal of Asian Earth Sciences*, 152, 12–22. doi: [10.1016/j.jseaes.2017.11.005](https://doi.org/10.1016/j.jseaes.2017.11.005)
- Norberg, U. M. (2002). Structure, form, and function of flight in engineering and the living world. *Journal of Morphology*, 252, 52–81. doi: [10.1002/jmor.10013](https://doi.org/10.1002/jmor.10013)
- Nudds, R. L., & Dyke, G. D. (2010). Narrow primary feather rachises in *Confuciusornis* and *Archaeopteryx* suggest poor flight ability. *Science*, 328, 887–889. doi: [10.1126/science.1188895](https://doi.org/10.1126/science.1188895)
- O'Connor, J. K., Chiappe, L. M., & Bell, A. (2011). Pre-Modern birds: avian divergences in the Mesozoic. In G. Dyke, & G. Kaiser (Eds.), *Living Dinosaurs: the evolutionary history of birds* (pp. 39–114). Wiley.
- O'Connor, J. K., Chiappe, L. M., Chuong, C., Bottjer, D., & You, H. (2012). Homology and potential cellular and molecular mechanisms for development of unique feather morphologies in early birds. *Geosciences*, 2, 157–177. doi: [10.3390%2Fgeosciences2030157](https://doi.org/10.3390%2Fgeosciences2030157)
- O'Connor, J. K. (2020). The plumage of basal birds. In C. Foth, & O. W. M. Rauhut (Eds.), *The evolution of feathers: from the origin to the present* (pp. 147–172). Springer Nature.
- Pan, Y., Zheng, W., Moyer, A., O'Connor, J. K., Wang, M., Zheng, X., Wang, X., Schroeter, E. R., Zhou, Z., & Schweitzer, M. H. (2016). Molecular evidence of keratin and melanosomes in feathers of the Early Cretaceous bird *Eoconfuciusornis*. *Proceedings of the National Academy of Sciences*, 113, e7900–e7907. doi: [10.1073/pnas.1617168113](https://doi.org/10.1073/pnas.1617168113)
- Pennycuik, C. J. (2008). *Modeling the flying bird*. Elsevier-Academic Press.
- Peters, D. S., & Ji, Q. (1999). Mußte *Confuciusornis* klettern? *Journal of Ornithology*, 140, 41–50.
- Peters, W. S., & Peters, D. S. (2009). Life History, sexual dimorphism and 'ornamental' feathers in the Mesozoic bird *Confuciusornis sanctus*. *Biology Letters*, 5, 817–822. doi: [10.1098%2Frsbl.2009.0574](https://doi.org/10.1098%2Frsbl.2009.0574)
- Pittman, M., Kaye, T. G., Wang, X., Zheng, X., Dececchi, T. A., & Hartman, S. A. (2022). Preserved soft anatomy confirms shoulder-powered upstroke of early theropod flyers, reveals enhanced early pygostylian upstroke, and explains early sternum loss. *Proceedings of the National Academy of Sciences*, 119(47), e2205476119.
- Rayner, J. M. (1988). The evolution of vertebrate flight. *Biological Journal of the Linnean Society*, 34, 269–287. doi: [10.1111/j.1095-8312.1988.tb01963.x](https://doi.org/10.1111/j.1095-8312.1988.tb01963.x)
- Rayner, J. M. (1999). Estimating power curves of flying vertebrates. *Journal of Experimental Biology*, 202, 3449–3461. doi: [10.1242/jeb.202.23.3449](https://doi.org/10.1242/jeb.202.23.3449)
- Rayner, J. M. (2001). On the origin and evolution of flapping flight aerodynamics in birds. In J. Gauthier, & L. F. Gall (Eds.), *New perspectives on the origin and early evolution of birds: proceedings of the international symposium in honor of John H. Ostrom* (pp. 363–385). Peabody Museum of Natural History, Yale University.
- Rosén, M., & Hedenström, A. (2001). Gliding flight in a jackdaw: a wind tunnel study. *Journal of Experimental Biology*, 204, 1153–1166. doi: [10.1242/jeb.204.6.1153](https://doi.org/10.1242/jeb.204.6.1153)
- Sachs, G. (2015). New model of flap-gliding flight. *Journal of Theoretical Biology*, 377, 110–116. doi: [10.1016/j.jtbi.2015.03.022](https://doi.org/10.1016/j.jtbi.2015.03.022)
- Schmidt-Nielsen, K. (1997). *Animal physiology: adaptation and environment*. Cambridge University Press.
- Senter, P. (2006). Scapular orientation in theropods and basal birds, and the origin of flapping flight. *Acta Palaeontologica Polonica*, 51, 305–313.
- Serrano, F. J., Palmqvist, P., & Sanz, J. L. (2015). Multivariate analysis of neognath skeletal measurements: implications for body mass estimation in Mesozoic birds. *Zoological Journal of the Linnean Society*, 173, 929–955. doi: [10.1111/zoj.12215](https://doi.org/10.1111/zoj.12215)

- Serrano, F. J., & Chiappe, L. M. (2017). Aerodynamic modeling of a Cretaceous bird reveals thermal soaring capabilities during early avian evolution. *Journal of the Royal Society Interface*, 14, 20170182. doi: [10.1111/zoj.12215](https://doi.org/10.1111/zoj.12215)
- Serrano, F. J., Palmqvist, P., Chiappe, L. M., & Sanz, J. L. (2017). Inferring flight parameters of Mesozoic avians through multivariate analyses of forelimb elements in their living relatives. *Paleobiology*, 43, 144–169. doi: [10.1017/pab.2016.35](https://doi.org/10.1017/pab.2016.35)
- Serrano, F. J., Chiappe, L. M., Palmqvist, P., Figueirido, B., Marugán-Lobón, J., & Sanz, J. L. (2018). Flight reconstruction of two European enantiornithines (Aves, Pygostylia) and the achievement of bounding flight in early cretaceous birds. *Palaeontology*, 61, 359–368. doi: [10.1111/pala.12351](https://doi.org/10.1111/pala.12351)
- Serrano, F. J., Chiappe, L. M., Palmqvist, P., Figueirido, B., Long, J., & Sanz, J. L. (2019). The effect of long-term atmospheric changes on the macroevolution of birds. *Gondwana Research*, 65, 86–96. doi: [10.1016/j.gr.2018.09.002](https://doi.org/10.1016/j.gr.2018.09.002)
- Taylor, G. K., & Thomas, A. L. (2014). *Evolutionary biomechanics: selection, phylogeny and constraint*. Oxford University Press.
- Taylor, G. K., Reynolds, K. V., & Thomas, A. L. (2016). Soaring energetics and glide performance in a moving atmosphere. *Philosophical Transactions of the Royal Society of London Series B*, 371, 20150398. doi: [10.1098/rstb.2015.0398](https://doi.org/10.1098/rstb.2015.0398)
- Tucker, V. A. (1973). Bird metabolism during flight: evaluation of a theory. *Journal of Experimental Biology*, 58, 689–709.
- Wang, L., Guo, Y., An, X., Zhao, Y., & Wang, J. (2019). Three-dimensional reconstruction and numerical simulation of flight performance of *Confuciusornis*. *Open Journal of Natural Sciences*, 7, 590–595.
- Wang, M., & Zhou, Z. (2018). A new confuciusornithid (Aves: Pygostylia) from the Early Cretaceous increases the morphological disparity of the Confuciusornithidae. *Zoological Journal of the Linnean Society*, 20, 1–14. doi: [10.1093/zoolinnean/zly045](https://doi.org/10.1093/zoolinnean/zly045)
- Wang, M., O'Connor J. K., & Zhou Z. (2018). A taxonomical revision of the Confuciusornithiformes (Aves: Pygostylia). *Vertebrata PalAsiatica*, 57, 1–37. doi: [10.19615/j.cnki.1000-3118.180530](https://doi.org/10.19615/j.cnki.1000-3118.180530)
- Wang, M., Stidham, T. A., Li, Z., Xu, X., Zhou, Z. (2021). Cretaceous bird with dinosaur skull sheds light on avian cranial evolution. *Nature Communications*, 12, 3890. doi: [10.1038/s41467-021-24147-z](https://doi.org/10.1038/s41467-021-24147-z)
- Wang, R., Hu, D., Zhang, M., Wang, S., Zhao, Q., Sullivan, C., & Xu, X. (2022). A new confuciusornithid bird with a secondary epiphyseal ossification reveals phylogenetic changes in confuciusornithid flight mode. *Communications Biology*, 5, 1398. doi: [10.1038/s42003-022-04316-6](https://doi.org/10.1038/s42003-022-04316-6)
- Wang, W., & O'Connor, J. K. (2017). Morphological coevolution of the pygostyle and tail feathers in early cretaceous birds. *Vertebrata PalAsiatica*, 55, 289–314. doi: [10.19615/j.cnki.1000-3118.170118](https://doi.org/10.19615/j.cnki.1000-3118.170118)
- Wang, X., McGowan, A. J., & Dyke, G. J. (2011). Avian wing proportions and flight styles: first step towards predicting the flight modes of Mesozoic birds. *PLoS One*, 6, e28672. doi: [10.1371/annotation/6c8c755f-58fc-49e3-b499-8d082318eef6](https://doi.org/10.1371/annotation/6c8c755f-58fc-49e3-b499-8d082318eef6)
- Ward, P., & Berner, R. (2011). Why were there dinosaurs? Why are there birds? In G. Dyke, & G. Kaiser (Eds.), *Living Dinosaurs: the evolutionary history of birds* (pp. 30–38). Wiley.
- Wellnhofer, P. (2009). *Archaeopteryx: The Icon of Evolution*. Verlag Dr. Friedrich Pfeil.
- Wu, Q., Bailleul, A. M., Li, Z., O'Connor, J. K., & Zhou, Z. (2021). Osteohistology of the scapulocoracoid of *Confuciusornis* and preliminary analysis of the shoulder joint in Aves. *Frontiers of Earth Sciences*, 9, 617124. doi: [10.3389/feart.2021.617124](https://doi.org/10.3389/feart.2021.617124)
- Xing, L., Cockx, P., Mckellar, R. C., & O'Connor, J. K. (2018). Ornamental feathers in cretaceous Burmese amber: resolving the enigma of rachis-dominated feather structure. *Journal of Palaeogeography*, 7, 13. doi: [10.1186/s42501-018-0014-2](https://doi.org/10.1186/s42501-018-0014-2)
- Zhang, F., Zhou, Z., & Benton, M. J. (2008). A primitive confuciusornithid bird from China and its implications for early avian flight. *Science China*, 51, 625–639. doi: [10.1007/s11430-008-0050-3](https://doi.org/10.1007/s11430-008-0050-3)
- Zheng, X., Xu, X., Zhou, Z., Miao, D., & Zhang, F. (2010). Comment on “Narrow primary feather rachises in *Confuciusornis* and *Archaeopteryx* suggest poor flight ability”. *Science*, 330, 320. doi: [10.1126/science.1193474](https://doi.org/10.1126/science.1193474)
- Zheng, X., Zhou, Z., Wang, X., Zhang, F., Zhang, X., Wang, Y., Wei, G., Wang, S., & Xu, X. (2013). Hind wings in basal birds and the evolution of leg feathers. *Science*, 339, 1309–1312. doi: [10.1126/science.1228753](https://doi.org/10.1126/science.1228753)
- Zhou, Z., & Farlow, J. O. (2001). Flight capability and habits of *Confuciusornis*. In J. Gauthier, & L. F. Gall (Eds.), *New perspectives on the origin and early evolution of birds: proceedings of the international symposium in honor of John H. Ostrom* (pp. 237–254). Peabody Museum of Natural History, Yale University.